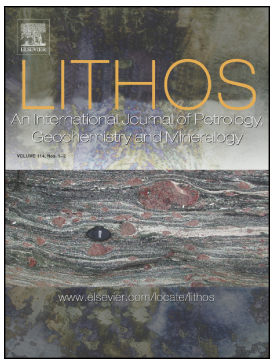

A HIMU volcanic belt along the SW African coast (~83–49 Ma): New geochemical clues to deep mantle dynamics from carbonatite and silica-undersaturated complexes in Namibia

H. Zhou, K. Hoernle, J. Geldmacher, F. Hauff, S. Homrighausen, D. Garbe-Schönberg, S. Jung, I. Bindeman

PII: S0024-4937(22)00248-1

DOI: https://doi.org/10.1016/j.lithos.2022.106839

Reference: LITHOS 106839

To appear in: *LITHOS*

Received date: 17 April 2022

Revised date: 7 August 2022

Accepted date: 10 August 2022

Please cite this article as: H. Zhou, K. Hoernle, J. Geldmacher, et al., A HIMU volcanic belt along the SW African coast (~83–49 Ma): New geochemical clues to deep mantle dynamics from carbonatite and silica-undersaturated complexes in Namibia, *LITHOS* (2022), https://doi.org/10.1016/j.lithos.2022.106839

A HIMU volcanic belt along the SW African coast (~83–49 Ma): New geochemical clues to deep mantle dynamics from carbonatite and silica-undersaturated complexes in Namibia

H.Zhou[a,e*], K.Hoernle[a, b], J.Geldmacher[a], F.Hauff[a], S.Homrighausen[a], D.Garbe-Schönberg[b], S. Jung[c], I. Bindeman[d]

[a]GEOMAR Helmholtz Centre for Ocean Research Kiel, Wischhofstr. 1-3, 24148 Kiel, Germany

[b]Institute of Geosciences, Kiel University, Ludewig-Meyn-Str. 10, 24118 Kiel, Germany

[c]Institute of Mineralogy and Petrography, Universität Hamburg, Grindelallee 48, 20146 Hamburg, Germany

[d]Department of Earth Sciences, University of Oregon, Eugene, OR, USA.

[e]Research Institute of Petroleum Exploration and Development, China National Petroleum Corporation, Beijing 100083, China

* Corresponding author. Email address: zhp_cn@hotmail.com

Abstract

The origin of carbonatitic and highly silica-undersaturated volcanism, common along the SW coast of Africa extending from Angola through Namibia to the tip of South Africa, is still poorly understood. Here we present new geochemical data (major and trace element and Sr-Nd-Pb-Hf-O-C isotopes) from the Agate Mountain calcio- to magnesio-carbonatites (~83 Ma), Dicker Willem calcio-carbonatites (49 Ma) and Swakopmund basanitic plugs (76-72 Ma) along the coast of Namibia that were emplaced after the EMI (enriched mantle one) type Etendeka flood basalts. The trace element and isotopic composition of Agate Mountain carbonatites and Swakopmund basanites indicate that they were derived from a HIMU-type (high time-integrated $^{238}U/^{204}Pb$ with radiogenic Pb isotope ratios) magma source, similar to the St. Helena global HIMU endmember in the South Atlantic. The Agate Mountain carbonatites form part of the late-stage Walvis Ridge HIMU hotspot track overlying the EM1-type Walvis Ridge basement forming part of the Tristan-Gough hotspot track. The Dicker Willem carbonatites, however, extend to higher $^{206}Pb/^{204}Pb$ than St. Helena, but have similar $^{206}Pb/^{204}Pb$ to Mangaia HIMU lavas in the Pacific. Compared to Mangaia HIMU, the Dicker Willem carbonatites with mantle-type O and C isotopes have higher $^{207}Pb/^{204}Pb$ and $^{87}Sr/^{86}Sr$ but lower $^{143}Nd/^{144}Nd$, suggesting it may represent a new HIMU endmember flavor. The HIMU carbonatitic and silica-undersaturated rocks form a belt of age-progressive volcanic tracks, including: 1) from the Walvis Ridge, through NW Namibia to central Angola, 2) from the Vema Seamount via Dicker Willem carbonatite to Gibeon kimberlites and carbonatites, 3) from the Warmbad to Bushmanland and to Namaqualand volcanic centers in northwestern South Africa, and 4) along the older end of the Shona EMI-type volcanic track extending into South Africa. Geochemical and seismic tomographic data suggest that the EMI and HIMU mantle plumes are generated from different

geochemical domains at the base of the lower mantle. The Tristan-Gough, Discovery and Shona EM1 volcanic tracks are derived from a common low-velocity anomaly (superplume-like structure with three branching arms) ascending from the outer margin of the African large low-shear-velocity province (LLSVP). Seismic low-velocity anomalies can be traced from beneath the belt of HIMU volcanism to an internal and shallower part of the LLSVP, located ~900–1200 km east of the outer LLSVP margin and suggest that HIMU-type material overlies EMI-type material in the internal part of the LLSVP.

Keywords: large low-shear-velocity province; EM1 mantle endmember; HIMU; Sr-Nd-Pb-Hf-O-C isotope geochemistry; Carbonatite

1. Introduction

The Sr-Nd-Hf-Pb isotopic composition of ocean island basalt (OIB) lavas show that at least four endmembers are required to explain the variations observed in Earth's mantle. These include: 1) the depleted mid-ocean-ridge-basalt (MORB) upper mantle source (DMM), 2) enriched mantle one (EM1) with radiogenic $^{87}Sr/^{86}Sr$, $^{207}Pb/^{204}Pb$ and $^{208}Pb/^{204}Pb$ but unradiogenic $^{143}Nd/^{144}Nd$, $^{176}Hf/^{177}Hf$ and $^{206}Pb/^{204}Pb$, 3) enriched mantle two (EM2), similar to EMI but with intermediate $^{206}Pb/^{204}Pb$ isotope ratios and less unradiogenic Nd and Hf isotope ratios, and 4) high time-integrated $^{238}U/^{204}Pb = \mu$ (HIMU) mantle with very radiogenic Pb isotope ratios (Castillo, 2015; Stracke et al., 2005 and references therein). A possible fifth common mantle component with high $^{3}He/^{4}He$ (>10) was termed PREMA and Focal Zone "FOZO" (Castillo, 2015, Stracke et al., 2005 and references therein). The type locality for the HIMU component in the Atlantic is St. Helena Island and in the Pacific is Mangaia Island (Stracke et al., 2005). St. Helena endmember type HIMU, however, has been identified globally (Homrighausen et al., 2018b). Unexpectedly, endmember St. Helena-type HIMU volcanism was recently found on the Walvis Ridge, the Atlantic type locality for the EM1 endmember, and the Shona hotspot track (Homrighausen et al., 2018a; Homrighausen et al., 2018b; Homrighausen et al., 2020) with a similar EMI-type endmember composition (Hoernle et al., 2016). These HIMU lavas are ~30 Ma younger than the underlying EMI-type basement at each respective location.

It has been shown that in order to generate endmember HIMU composition at least 1 Ga are required (Castillo, 2015; Homrighausen et al., 2018b; Stracke et al., 2005). Where endmember HIMU is stored within the mantle is controversial. Three potential mantle reservoirs, where the HIMU source material could have been isolated since the Archean, are: (1) shallow reservoir = the

subcontinental lithospheric mantle (SCLM; Rooney et al., 2014), 2) intermediate depth reservoir = the transition zone located between the upper and lower mantle (Mather et al., 2020 and references therein), and 3) deep reservoir at the base of lower mantle = Large Low-Shear Velocity Province (LLSVP) (Homrighausen et al., 2020 and references therein).

Here we present new geochemical (major and trace element and Sr-Nd-Pb-Hf-O-C isotope) data from two carbonatite complexes (Agate Mountain and Dicker Willem) and a basanite complex (Swakopmund plugs) along the Atlantic coast of Namibia (Figure 1). Combined with published data from the Vema Seamount, Gibeon carbonatite/kimberlite province, Walvis Ridge, Mocamedes Arch silica-undersaturated and carbonatitic complexes, Shona hotspot track, and the Warmbad, Bushmanland and Namaqualand clusters, we show that there is a broad belt of HIMU volcanism along the coast of southwest Africa, extending from the SW tip of South Africa to St. Helena Island. Volcanism at different locations along the N-S HIMU belt, generally belong to age-progressive tracks that get older to the NE (direction of plate motion). We combine these findings with seismic tomographic profiles that show 1) plume-like low-velocity anomalies under each of the EMI-type hotspots (Tristan-Gough, Discovery and Shona) that coalesce in the transition zone and extend down to the western margin of the African LLSVP (possibly representing a super plume branching out in the transition zone), and 2) multiple, more discontinuous low-velocity anomalies extending beneath the belt of HIMU volcanism to an internal, shallower portion of the LLSVP, consistent with a layered LLSVP (HIMU layer overlying EMI layer).

2. Geological background and previous research

2.1. General background

On the African plate, several age-progressive hotspot tracks, including Tristan-Gough, Discovery and the Shona track (Figure 1), are proposed to be generated from mantle plumes derived from the SW margin of the African LLSVP (Homrighausen et al., 2019). Lavas forming these hotspot tracks have EM1-type geochemical compositions, characterized by radiogenic $^{87}Sr/^{86}Sr$ and $^{208}Pb/^{204}Pb$ but relatively unradiogenic $^{143}Nd/^{144}Nd$ and $^{206}Pb/^{204}Pb$ (Class and le Roex, 2011; Homrighausen et al., 2019). Recently it was shown that the Tristan-Gough hotspot track is isotopically zoned over the last ≥70 Ma (Hoernle et al., 2015; Rohde et al., 2013). It consists of two sub-tracks (Figure 1): 1) a northern Tristan sub-track with Tristan-type composition (northern part of the SW Walvis Ridge, including DSDP Sites 527 and 528, and the part of the seamount chain that leads to Tristan Island), and 2) a southern Gough sub-track with Gough-type composition (NE two thirds of the Walvis Ridge, southern portion of SW end of the Walvis Ridge, including DSDP Site 525A, and southern part of the Guyot Province that extends to Gough Island). Both the Tristan and Gough sub-tracks have EM1-type geochemical compositions, but the Gough component possesses higher $^{207}Pb/^{204}Pb$ but similar $^{208}Pb/^{204}Pb$, Sr, Nd, Hf isotope ratios at a given $^{206}Pb/^{204}Pb$ ratio compared to the Tristan component (Hoernle et al., 2015; Homrighausen et al., 2019; Rohde et al., 2013).

Consistent with the classic plume head – plume tail model (Richards et al., 1989), the Tristan-Gough and Shona hotspot tracks appear to have initiated with flood basalt events: the Etendeka/Parana (~132 Ma) and Karoo (~180 Ma) flood basalt events, respectively (e.g., Homrighausen et al., 2020). Accordingly, the Tristan-Gough plume head trigged widespread flood basalt volcanism in Namibia

(Etendeka) and the conjugate South America margin (Paraná), contemporaneous with breakup between Africa and South America (O'Connor and le Roex, 1992). The Etendeka flood basalts contain two dominant components: High-Ti tholeiitic basalts with a Gough-type isotopic composition and low-Ti tholeiitic basalts that have a more depleted composition, similar to Atlantic MORB except for higher $^{207}Pb/^{204}Pb$ at a given $^{206}Pb/^{204}Pb$ isotope ratio (Trumbull, 2004; Zhou et al., 2020). Younger (~130-120) silica-undersaturated and carbonatitic centers, such as Messum, Okenyenu and Ondurakorume, have similar isotopic compositions to Etendeka flood basalts and are also interpreted to ultimately be derived from the Tristan-Gough plume head (Le Roex and Lanyon, 1998). High $^{3}He/^{4}He$ isotope ratios have recently been found in high-forsteritic olivine in the low-Ti basalts, pointing to derivation from the lower mantle (Stronik et al., 2017). The Discovery hotspot track lavas to the south of Gough Island also have an EM1-type composition with the northern Discovery seamounts similar to the Gough-type sub-track lavas and the southern Discovery seamounts having even more extreme EMI-like compositions (Schwindrofska et al., 2016), whereas the Shona track, still further south, consists almost exclusively of the Gough-type composition (Hoernle et al., 2016) (Figure 1). Therefore, Gough-type EM1 is the dominant flavor found in the three aforementioned South Atlantic hotspots (Tristan-Gough, Discovery and Shona) and the Etendeka flood basalts. Associated geochemical anomalies at the South Atlantic mid-ocean ridge reveal that the northern (Gough-type composition) Discovery and Shona domains have high $^{3}He/^{4}He$ and primitive Ne isotopic compositions, consistent with a lower mantle origin for the Gough-type composition (Sarda et al., 2000), as was the case for the depleted low-Ti Etendeka melts.

Recently, secondary age-progressive volcanic tracks with St. Helena-type HIMU composition were discovered superimposed on and adjacent to the EM1 Walvis Ridge and Shona volcanic tracks

(Homrighausen et al., 2018a; Homrighausen et al., 2020). Ar/Ar age dating showed that these low-volume HIMU lavas erupted ~30 Ma after the EMI-type volcanism at any given site on both hotspot tracks. It was proposed that the HIMU volcanism was derived from secondary plumes that upwelled 900–1200 km northeastwards (in the direction of plate motion) of the main Tristan-Gough and Shona plumes, thus sampling an internal part of the African LLSVP, which has a HIMU-type composition (Homrighausen et al., 2020). The small-scale HIMU secondary plumes were presumably triggered by the removal of large amounts of EMI material from the LLSVP margin by the starting plume heads of the Tristan-Gough and Shona hotspots that generated the Etendeka/Parana and the Karoo flood basalts. Chauvel et al. (2012) also proposed that HIMU plumes could be generated from internal portions of LLSVPs. Ballmer et al. (2016) suggested a layered LLSVP based on seismic velocity data and numerical models with recycled "basaltic" material overlying a primitive or primordial layer. Seismic tomography shows a steep internal slope/step ~900–1200 km northeastwards of the outer LLSVP margin, which has been interpreted as the generation zone for the secondary HIMU plumes (Homrighausen et al., 2020).

Young (relative to Etendeka) low-volume alkalic-carbonatitic igneous centers also occur on the west coast of Namibia (e.g., Homrighausen et al., 2020; Reid et al., 1990; Whitehead et al., 2002 and references therein). These centers include Agate Mountain, the alkaline plugs near Swakopmund, Dicker Willem and the Gibeon kimberlite-carbonatite complexes. An important question is whether these volcanic centers are derived from EMI (Etendeka) or HIMU-type sources and what the relationship between these two chemically distinct type sources is.

2.2. Carbonatites

Although carbonatites only make up a tiny fraction of Earth's crustal rocks, their unusual composition, debated origin and significance as metallic resource deposits makes them particularly interesting for geochemical investigations. Carbonatites and associated alkaline rocks are the most important source of economically exploitable rare earth elements (REE) and Nb, with >98% of mine production of Nb being from carbonatite (U.S. Geological Survey). While REEs, Nb and Ta are essential for the advanced digital and green high technology applications, the composition and origin of carbonatites need to be elucidated in order to better understand where carbonatites can be found and what kinds of carbonatites contain the highest abundances of economically important metals.

Carbonatites and associated silica-undersaturated magmatism are believed to form by very low degrees of melting (Gudfinnsson and Presnall, 2005) of carbonated peridotite (Dasgupta and Hirschmann, 2006) or eclogite/pyroxenite (Dasgupta et al., 2007). Depending on source composition, temperature and pressure, both calcio- and magnesio-carbonatites can form through melting of mantle rocks (Weidendorfer et al., 2020). With increasing degree of melting, a series of carbonatite to silica-undersaturated rocks (carbonatites, kimberlites, nephelinites, basanites and alkali basalts) can be generated from the same mantle source (Dasgupta et al., 2007; Gudfinnsson and Presnall, 2005). In addition, experimental studies show that CO_2 plays an important role in the melting of mantle rocks to generate highly silica-undersaturated compositions (Dasgupta and Hirschmann, 2006; Gudfinnsson and Presnall, 2005).

2.3. Agate Mountain Carbonatite Complex

The Agate Mountain carbonatite complex is located in northwestern Namibia on the continental extension of the Walvis Ridge (Figure 1). It was geologically mapped by Miller (2000) (Figure 2a). The complex is intruded into the surrounding Proterozoic Kaoko Belt, the Cretaceous Khumib formation tholeiitic lavas and the Skeleton Coast quartz latite sub-group of the Etendeka flood basalt event (Marsh et al., 2001). Therefore, the carbonatite complex must be younger than the ~130 Ma Etendeka volcanism. Based on seismic data, Agate Mountain appears to be a satellite center of a much larger (now largely offshore) volcanic complex (Phoenix Volcano; Miller, 2008). The age of the Phoenix Volcano has been bracketed using seismic reflection data to have formed within the Turonian and Campanian (between 93.5–81 Ma; Baby et al., 2018). The Agate Mountain carbonatite complex is composed of two domains, separated by ring faults: 1) main body of the carbonatite complex, filling the center of the ring structure, and 2) predominantly fenite and fenitized Etendeka quartz latite from the intrusive carbonatite forms the outer ring structure, preserved west of the mountain's summit (Miller, 2008). The carbonatites and alkaline rocks investigated in this study were sampled from dikes and scattered plugs in the center of the complex and adjacent to the Khumib basaltic lavas (Figure 2a). Although it has not been possible to date the carbonatites directly, phonolite plugs and dikes, emplaced contemporaneously and/or after the carbonatitic plugs (Miller et al., 2008), have been dated at 83–82 Ma (Homrighausen et al., 2020). Therefore, we assume an age of ~83 Ma for the complex, which is consistent with the carbonatites belonging to a satellitic vent on the Turonian-Campanian Phoenix Volcano. The phonolites have a HIMU-type isotopic composition (Homrighausen et al., 2020) (Figure 2a).

2.4. Alkaline plugs near Swakopmund

A cluster of intrusive alkaline plugs, about 17km east of Swakopmund in western central Namibia (Figure. 2b), was first described by Whitehead et al. (2002). The exposed plugs on both sides of the road from Swakopmund to Usakos form up to 25m high hills in the eroded Proterozoic Damara Belt rocks. Previously, major and trace element data were published for two basanites (see Figure 3b; termed nephelinites in Whitehead et al., 2002) and for a phonolitic sample from these plugs. Two Ar-Ar whole-rock ages (76.08 ± 0.86; 74.86 ± 0.92 Ma) from basanite samples were reported in Whitehead et al. (2002), but no further details of the age measurements were published. A slightly younger pseudo plateau age of 72.50±0.47 Ma from sample NAM61 collected north of the Swakop River, for which we provide geochemical data in this study, has also been published (Homrighausen et al., 2020). No isotope data were published from these plugs thus far. Samples for this study are taken from the two plugs north of the Swakop river and the road from Usakos to Swakopmund (Figure 2b).

Although the overall volume of the plugs is small, their abundant lherzolite xenoliths have been used to constrain the composition of the SCLM beneath the Damara Belt (Whitehead et al., 2002). Accordingly, Swakopmund lherzolite xenoliths show very low $^{87}Sr/^{86}Sr_{70Ma}$ (0.70237–0.70250) and high $^{143}Nd/^{144}Nd_{70Ma}$ (0.51318–0.51320) ratios, and thus show no signs of either Etendeka EMI or HIMU-type influence but rather indicate a depleted SCLM beneath the Swakopmund intrusions (Class and le Roex, 2006).

2.5. Dicker Willem

Dicker Willem stands out as an inselberg in SW Namibia (Figure 2c). It consists mainly of carbonatitic magma intruded into the surrounding 1.0–1.3 Ga old Namaqua Metamorphic Complex (Miller, 2008).

With an age of 49±1 Ma constrained by K-Ar and Rb-Sr dating (Reid et al., 1990), Dicker Willem is significantly younger than the Etendeka flood basalt episode and the initiation of the Walvis Ridge hotspot track. Cooper (1988) classified the carbonatites of Dicker Willem as sövites, alvikites, beforsites, ferro-alvikites and also described dikes of carbonatite, microbreccia and tuffisite. The major and trace element variation of the carbonatitic rock types is attributed to the continuous fractionation of a common parental magma (Cooper and Reid, 1998). Sövites form the outer margin as an intermittent concentric ring and can be coherently traced along the northeastern and southern flanks of Dicker Willem. Ijolite-syenite xenoliths occur within the sövites and are likely to be related to the carbonatites (Cooper, 1988). The center of the Dicker Willem complex is formed by alvikites. Sövite dikes and veins are the latest intrusions at Dicker Willem, occurring both within and outside of the complex. The carbonatites for this study are taken from the sövite ring on the southern slope and the alvikitic center (Figure 2c). One phonolite was taken from the trachyte breccia at the southeastern flank, which is also described in Cooper (1988). Published isotope data from Dicker Willem show a wide range between a HIMU endmember and the local upper crust Namaqua gneiss composition (Cooper and Reid, 2000).

3. Samples, petrography and analytical methods

The exact coordinates of all collected samples are given in Appendix A.

Our carbonatite samples from Agate mountain are divided into sövites and alvikites by their grain size (Le Maitre et al., 2005). The sövite dike rocks contain up to 30% quartz, radiating clusters of opaque minerals and skeletal crystals of dolomite (0.2–0.4 mm). Similar petrographic features were also described by Miller (2000). Alvikites are fine grained and contain Fe oxides and quartz. Some

carbonatite dike samples contain more accessory minerals, such as nepheline, fluorite, melilite, clusters of aegirine, phlogopite and opaque ore.

Dicker Willem samples consist of sövite, alvikite and silicate rocks. The sampled sövite rocks mainly contain up to 4 mm large anhedral calcite and accessory minerals such as biotite (0.05–0.4 mm), apatite (~0.2 mm), aegirine (~2 mm) and magnetite (~5 mm). Alvikites have a typical calcitic groundmass and varying contents of opaque Fe-oxide minerals. The phonolite contains alkali feldspar, nepheline, aegirine and alkali amphibole. The matrix consists largely of calcite, which is similar to strongly-altered trachyte breccia described by Cooper (1988).

The basanite plugs sampled near Swakopmund are aphyric to sparsely porphyric with 10–20% olivine and augite phenocrysts (~0.5mm). The matrix consists of feldspathoid and Fe-Ti oxide microphenocrysts (0.03–0.05 mm). The rocks contain abundant lherzolite and rare harzburgite xenoliths, as previously reported by Whitehead et al. (2002). The xenoliths have a holocrystalline texture with anhedral olivine, clinopyroxene and rare spinel (0.4–2 mm) but no garnet. The xenolith suite thus appears to belong to the spinel facies, consistent with an origin from the lithospheric mantle (Whitehead et al., 2002).

The sample material was crushed in a jaw crusher, cleaned in an ultrasonic bath with deionized water, sieved and carefully hand-picked under a binocular microscope to avoid secondary fillings of cavities/ fractures and xenolithic material. Selected whole-rock chips (~10g) of each sample were milled to fine powders and dried at 105°C overnight.

Major elements of most samples (see Appendix A) were measured at the Institute of Mineralogy and Petrography at the University of Hamburg on a Magix Pro PW 2540 X-ray fluorescence spectrometer

(XRF). International rock standards JGB-1, JB-3, JB-2, JA-3, JG-3, JG-2 were analyzed together with the samples. The difference between measured and accepted literature values (Govindaraju, 1994) of major elements is less than 7%, except for elements with mass fractions lower than 1 wt%. Since eight carbonatites possess high concentrations of Sr and Ba (higher concentrations than covered by the calibration curve and thus yielding high analytical errors when measured by XRF), the major element composition of these samples was determined by inductively coupled plasma optical emission spectrometry (ICP-OES) on a SPECTRO CIROS SOP at the Institute of Geosciences at Kiel University. The reference standards MACS-3 (Jochum et al., 2019) and COQ-1 (Ray et al., 2013) were measured together with samples. The difference between measured and literature values are less than 6%, except for elements with mass fractions lower than 1 wt%. The precision of ICP-OES measurements based on duplicate measurements is better than 5%.

Trace elements were determined with an AGILENT 7500cs inductively coupled plasma mass spectrometer (ICP-MS) at the Institute of Geosciences at Kiel University. Carbonatites were decarbonized by diluted hydrochloric acid. Then rock powders (~100 mg) were treated with HF-$HClO_4$-aqua regia following the standard decomposition procedure of Garbe-Schönberg (1993). The carbonatitic powders, however, could not be fully dissolved by this method. Therefore, these samples were milled to nano-particulate powders and measured by laser ablation inductively coupled plasma mass spectrometer (LA-ICP-MS). About 2g powder for each sample was milled with 8 ml deionized water for 3 min in a planetary mill at 700–800 rpm. All samples were then carefully rinsed into polycarbonate beakers and freeze-dried. After 5 minutes of re-homogenization, about 300 mg powder were pressed into tablets under 0.74×10^6 kPa (Garbe-Schönberg and Müller, 2014). The tablets were measured by Agilent 7900 ICP-MS coupled with a GeoLas HD (Coherent) 193 nm

ArF excimer laser ablation system at Kiel University. Every tablet was measured three times and the average value is reported. The uncertainty combines both the uncertainty from the measurement (including slightly higher variability of aerosol generation during laser ablation of nano-powder) and the uncertainty from any remaining heterogeneity of the tablet. Most RSD%s (relative standard deviations) of replicates are lower than 5%, except for elements with lower than 1 µg/g concentrations. A carbonatite standard (MACS-3 NP) was measured together with the nano-powder tablets. The difference between measured and literature data (Jochum et al., 2019) is less than 8%, except for Mn, Fe, Rb, Zr, Sr.

Carbon and oxygen isotopes were measured at the University of Oregon using a Gasbench continuous flow line coupled with a Thermo-Finnigan MAT253 gas isotope ratio mass spectrometer. The freshest carbonate minerals (0.4 mg) were ground and put into 10 ml vials, which were flushed with He, then acidified with phosphoric acid inside of a thermal block held at 70°C. After equilibration for 2 h, the samples were run sequentially, and an analysis run included the NBS19 standard and in house carbonatite standard MCA. Carbon isotope values are reported relative to the PDB standard. The NBS19 standard yielded $\delta^{13}C$ =2.09±0.032‰ PDB (2SE). Oxygen isotope values are reported relative to the international Vienna Standard Mean Ocean Water (VSMOW) standard. The measured $\delta^{18}O$ values of NBS19 are 28.03±0.057 (2SE). The analytical values were adjusted by the difference between our measured and recommended values for the respective standards (0.14 for $\delta^{13}C$ and -0.61 for $\delta^{18}O$).

The Sr-Nd-Pb isotope ratios were measured at the GEOMAR Helmholtz Centre for Ocean Research Kiel by thermal ionization mass spectrometry (TIMS) using a Thermo-Scientific TRITON *Plus*. About 20–30 mg powders were dissolved by HF-HNO_3. The sample solutions were then passed through ion

chromatographic columns following the procedures described in Hoernle et al. (2008). The Sr and Nd isotopic ratios were fractionation-corrected within-run to $^{86}Sr/^{88}Sr = 0.1194$ and $^{146}Nd/^{144}Nd = 0.7219$. NBS987 and La Jolla reference materials were measured 4 to 5 times along with the samples on each turret. The average of measured $^{87}Sr/^{86}Sr$ (NBS987) and $^{143}Nd/^{144}Nd$ (La Jolla) were normalized to 0.710250 and 0.511850 respectively for each turret and the normalization value applied to the sample data. This procedure compensates for long-term drift of the TIMS due to progressive degradation of faraday cups. Normalized NBS987 and La Jolla were reproduced at ± 0.000007 (n = 66, 2SD) and 0.000006 (n = 59, 2SD) respectively. Pb isotopes were measured using the double-spike (Pb-DS) technique (Hoernle et al., 2011). The DS corrected NBS981 values since the 2014 installation of the instrument are $^{206}Pb/^{204}Pb = 16.9408 \pm 0.0029$ $^{207}Pb/^{204}Pb = 15.4975 \pm 0.0019$, $^{208}Pb/^{204}Pb = 36.7207 \pm 0.0050$ (n=215; 2SD). Duplicate analysis of separate digestions lie within the above stated 2SD's of reference materials for NMH1 and NM9B. The same applies for $^{87}Sr/^{86}Sr$, $^{143}Nd/^{144}Nd$ and $^{207}Pb/^{204}Pb$ in triplicate digestions of NMH2 and NMH4 but $^{206}Pb/^{204}Pb$ (NMH2) and $^{208}Pb/^{204}Pb$ (NMH2 and NMH4) are slightly outside 2SD of NBS981 (see Appendix A for details). These variations are ascribed to variable U/Pb and Th/Pb domains that appear heterogeneously distributed in the sample powder. Unleached powders (200–300 mg) were prepared for Hf isotope measurements following the method of Blichert-Toft et al. (1997). Hf isotope ratios were also measured at GEOMAR on a NU MC-ICP-MS and sample data were fractionation-corrected by the standard bracketing method. The in-house standard SPEX Hf ICP solution (lot#9) yielded $^{176}Hf/^{177}Hf = 0.282170 \pm 0.000005$ (n=13; 2SD) corresponding to a JMC457 value = 0.282163 (Blichert-Toft et al., 1997). Procedural blanks were <30pg for Pb and <100pg for Sr-Nd-Hf.

4. Results

4.1. Major and trace element data

Major and trace element data are presented in Appendix A. The carbonatites show large variations in CaO (22.5–56.4 wt%), MgO (0–13.4 wt%), Fe_2O_3 (0–8.3 wt%) and SiO_2 (0–43.8 wt.%). All carbonatites have extremely low TiO_2 concentrations (0–0.22 wt%). Such low TiO_2 has been reported for carbonatites world-wide (e.g. Cooper and Reid, 1998; Hoernle et al., 2002). Following the classification of Le Maitre et al. (1989), carbonatites can be divided into three groups based on their Ca, Mg and Fe + Mn contents (Figure 3a). Accordingly, most of the sampled carbonatites are classified as calcio-carbonatite (> 80% CaO) but four samples from Agate Mountain are magnesio-carbonatites and two samples plot on the calcio-/ferro-carbonatite boundary. In comparison to oceanic carbonatites from ocean islands, the Namibian carbonatites have less sövitic compositions and trend towards lower CaO concentrations but higher SiO_2 (Figure 3 c and d). CaO content is generally negatively correlated with SiO_2.

As is characteristic for carbonatitic rocks, most samples have high Ba, Sr, Th, Pb and rare earth element (REE) concentrations, highly variable Nb, and are depleted in several high field strength elements (HFSE) (Ta, Hf, Zr, Ti), as well as in U and Rb, resulting in highly spiked patterns on standard multi-element diagrams (Figure 4a–c). Considering trace elements, no principal difference between calcio- and magnesio-carbonatites is obvious in our sample set (compare Figure 4a and b). Three secondary vein samples (NM10, NM18, NM27A, indicated in Figure 4) display significantly lower incompatible trace element abundances than typical carbonatites and are indicated in the figures by a distinct symbol. Element pairs with similar partition coefficients in silicate melts, such as Nb-Ta and Zr-Hf (and therefore generally similar normalized abundances), are decoupled in carbonatitic rocks.

Thus, the Nb/Ta ratios of the investigated carbonatites (13–6735) are much higher than the (silicate) chondritic value (19.9±0.6; Münker et al., 2003). Zr/Hf also varies considerably (19 to 303; with chondritic value being 34.3±0.3; Münker et al., 2003).

Compared to carbonatites from Bayan Obo (Inner Mongolia), the largest REE mine of the world (Yang et al., 2011), our Agate Mountain carbonatites have slightly higher average Nb (173 µg/g compared to 160 µg/g in Bayan Obo) and significantly higher HREE contents (total HREE concentration from Tb to Lu is 129 µg/g compared to 72 µg/g). In contrast, the total LREE concentrations of Agate Mountain carbonatites (6456 µg/g) and Dicker Willem (1893 µg/g) are much lower than in Bayan Obo (28900 µg/g).

The sampled silicate rocks range from basanite to benmoreite to phonolite on the total alkali vs. silica diagram (Figure 3b). All samples from the Swakopmund plugs have basanitic compositions in accordance with two previously published samples from these outcrops (Whitehead et al., 2002). In contrast, the sampled silicates from Agate Mountain and Dicker Willem are more differentiated and range from benmoreitic to phonolitic compositions.

On multi-element diagrams, Swakopmund basanites show uniform patterns with enrichment of more incompatible over less incompatible elements, enrichment in Nb, Ta, and depletion in K, Pb, Ti and steep negative HREE patterns (Figure. 4d). These patterns resemble typical HIMU-type OIB trace element patterns as shown by basanites from the St. Helena Island type locality in the South Atlantic (Chaffey et al., 1989).

4.2. Isotope data

The results of the isotope measurements are also presented in Appendix A. Oxygen and carbon isotope ratios are plotted in Figure 5. All radiogenic isotope ratios were corrected for radiogenic ingrowth to 70 Ma, which is the average age of Agate Mountain (82-84 Ma), Dicker Willem (49 Ma) and Swakopmund plugs (72-76 Ma) (Figure 6 and 7; see figure caption for further details).

The investigated carbonatites show a large range in $\delta^{18}O$, with most samples having higher $\delta^{18}O$ (>10‰) but $\delta^{13}C$ similar to primary (mantle-derived) carbonatites (Figure 5). Five carbonatites show slightly higher $\delta^{13}C$ (>-3‰). Two samples from Dicker Willem (NMH2 and NMH4) fall within the commonly accepted range of primary mantle-derived $\delta^{13}C$ and $\delta^{18}O$ values of -7 to -5‰ and 5 to 8‰, respectively (Keller and Hoefs, 1995). Neither $\delta^{18}O$ or $\delta^{13}C$ correlate with radiogenic isotope ratios, suggesting that the radiogenic isotope composition is not related to alteration or crustal assimilation.

The analyzed carbonatites show a large range in initial Sr isotope ratios (0.7032 to 0.7066) but fairly restricted initial Nd isotope ratios (0.51262 to 0.51276) largely overlapping the St. Helena HIMU composition (Figure 6a). The Swakopmund basanites show a much smaller spread of their initial Sr isotope ratios (0.70307 to 0.70406), largely overlapping with the Walvis Ridge HIMU silicates except for sample NM2018A, which yields $^{86}Sr/^{86}Sr_{in}$ of 0.7041. Initial Pb isotope compositions of carbonatites from the Agate Mountain complex range from moderately radiogenic ratios ($^{206}Pb/^{204}Pb_{70Ma}$=19.14, $^{207}Pb/^{204}Pb_{70Ma}$=15.69, $^{208}Pb/^{204}Pb_{70Ma}$=39.08, sample NM26B) to very radiogenic signatures ($^{206}Pb/^{204}Pb_{70Ma}$=20.66, $^{207}Pb/^{204}Pb_{70Ma}$=15.83, $^{208}Pb/^{204}Pb_{70Ma}$=40.13, sample NM24), which are similar to St. Helena end member HIMU-type lavas ($^{206}Pb/^{204}Pb_{70Ma}$=19.47–20.84, $^{207}Pb/^{204}Pb_{70Ma}$=15.64–15.95, $^{208}Pb/^{204}Pb_{70Ma}$=39.01–40.35; Chaffey et al., 1989) (Figure 7). Sample

NM10, a secondary silicate vein with depleted trace element composition (Figure 4b), yields distinctly less radiogenic Pb isotopes ($^{206}Pb/^{204}Pb_{70Ma}$=17.61, $^{207}Pb/^{204}Pb_{70Ma}$=15.55, $^{208}Pb/^{204}Pb_{70Ma}$=38.55), plotting in/near the field for high-Ti Etendeka basalts (also in the Sr vs Nd isotope diagram of Figure 6). This sample comes from a vein cutting the Etendeka basalts (high-Ti Khumib formation) east of Agate Mountain and has obviously picked up the isotopic composition of its host rock, which is completely distinct from the Agate Mountain carbonatites (see Figure 2a and Section 2.2).

Our Dicker Willem carbonatite samples display a relatively restricted range in $^{206}Pb/^{204}Pb_{70Ma}$ (20.50–21.66), $^{207}Pb/^{204}Pb_{70Ma}$ (15.80–15.88), $^{208}Pb/^{204}Pb_{70Ma}$ (39.78–40.09), $^{87}Sr/^{86}Sr_{70Ma}$ (0.7032–0.7034) and $^{143}Nd/^{144}Nd_{70Ma}$ (0.51266–0.51269), except for one sample (NMH1) with slightly more enriched $^{87}Sr/^{86}Sr_{70Ma}$ (0.70383) and $^{143}Nd/^{144}Nd_{70Ma}$ (0.51262). Its $^{206}Pb/^{204}Pb_{70Ma}$ (20.27) isotope ratio is lower, but $^{207}Pb/^{204}Pb_{70Ma}$ and $^{208}Pb/^{204}Pb_{70Ma}$ are similar to the other samples. The Nd isotope ratios of Dicker Willem carbonatites are slightly lower than the Agate Mountain and Swakopmund samples at a given Sr isotope ratio (Figure 6a). Previously published isotope data from Dicker Willem ($^{87}Sr/^{86}Sr_{70Ma}$ = 0.7032–0.7710; $^{143}Nd/^{144}Nd_{70Ma}$ = 0.51178–0.51269; $^{206}Pb/^{204}Pb_{70Ma}$ = 18.59–20.97) (Cooper and Reid, 2000, Cooper and Reid, 1998) extend to much more radiogenic Sr and unradiogenic Nd isotopic composition, likely reflecting greater amounts of bulk crustal assimilation than in the samples that we collected for this study (see Section 5.1 below). The Sr-Nd-Pb isotope replicates of NMH2 and NMH4 give similar results. Most measured isotope ratios are within the analytical errors (2SE) of each other.

The Swakopmund basanite plug lavas also have radiogenic Pb isotope ratios ($^{206}Pb/^{204}Pb_{70Ma}$ = 19.71–20.16; $^{207}Pb/^{204}Pb_{70Ma}$ = 15.70–15.72, $^{208}Pb/^{204}Pb_{70Ma}$ = 39.39–39.76) and have systematically lower

$^{207}Pb/^{204}Pb$ for a given $^{206}Pb/^{204}Pb$ than the carbonatite samples. When considering their combined Sr, Nd and Hf isotope ratios, the basanites largely overlap the composition of the late-stage HIMU seamounts on Walvis Ridge (Figure 6–7).

Overall, the Pb isotope ratios of the Agate Mountain carbonatites and silica-undersaturated volcanic rocks largely overlap with the Walvis Ridge HIMU and St. Helena HIMU compositions, and form good linear trends ($^{206}Pb/^{204}Pb$ vs. $^{207}Pb/^{204}Pb$, r^2=0.99; and vs. $^{208}Pb/^{204}Pb$, r^2=0.85) between the St. Helena HIMU endmember and the high-Ti Etendeka silicate rocks (Figure 7a, b). The two Dicker Willem carbonatites with mantle-like O and C isotopes, however, have higher $^{206}Pb/^{204}Pb_{in}$ and lower $^{143}Nd/^{144}Nd_{in}$ than St. Helena basanite lavas or Agate Mountain carbonatites.

5. Discussion

5.1. Alteration and crustal contamination

A potential problem with carbonatites is alteration and recrystallization. The Agate Mountain carbonatite complex is heavily eroded and it is located in a remote desert region without any fresh outcrops. Although most of the samples have C isotopic compositions consistent with a mantle composition, the elevated $\delta^{18}O$ suggests that the carbonatites have undergone low-temperature alteration (Figure 5). Two samples from the Dicker Willem carbonatite complex, however, have mantle-like O and C isotope ratios, plotting within the field for oceanic basalts and primary carbonatites from Keller and Hoefs (1995). Several samples from Agate Mountain and Dicker Willem have elevated $\delta^{18}O$ and $\delta^{13}C$, which could reflect high-temperature alteration or carbonate sediment assimilation. The two Dicker Willem samples with elevated O and C isotope values, however, have the lowest initial Sr isotope ratios, and thus show no clear evidence of crustal assimilation. The two

samples with the highest initial Sr isotope ratios also have high $\delta^{18}O$, suggesting that low-T alteration may have resulted in some exchange of Sr in the carbonatites with crustal Sr, despite the high Sr concentration in most carbonatites. The Swakopmund basanite samples have very similar concentrations of incompatible trace elements except for sample NM2018B, which has higher concentrations of all incompatible elements than the other samples except for TiO_2. Alteration appears to have had little effect on these samples.

Unlike magmas erupted in ocean basins such as the late-stage Walvis Ridge HIMU seamounts, magmas forming Agate Mountain, Dicker Willem and the Swakopmund plugs had to pass through thick Proterozoic continental crust with extreme trace element and isotopic composition. In particular, continental crust is characterized by high abundances of highly incompatible elements (such as the large ion lithophile elements and Pb) and by low relative abundances of Nb and Ta (Hofmann, 1988). The high concentration of incompatible elements in carbonatites and silica undersaturated rocks, however, makes any recognition of crustal contamination based solely on trace element content very difficult.

To comprehensively evaluate any crustal influence on silicate and carbonatitic rocks, we also evaluate their isotopic signatures. Sr isotope ratios are widely used in evaluating the crustal contamination of basaltic rocks, due to the extreme differences in $^{87}Sr/^{86}Sr$ between the mantle, such as 0.7025–0.7035 for upper mantle MORB source and up to ~0.7060 for intraplate ocean island basalts (OIBs) (Figure 6a), compared with the regional (upper) continental crust ($^{87}Sr/^{86}Sr_{70\ Ma}$ = 0.71–0.88, for Nama group and Kuiseb, Khan, Etusis formation metasedimentary rocks; McDermott and Hawkesworth, 1990). The Sr isotope ratios of calcio-carbonatites, however, are generally considered to be largely resistant to significant crustal contamination, because of their high natural Sr

concentration (e.g. Hoernle et al., 2002). Excluding the secondary silicate and carbonate veins (NM10, NM18 and NM27A) with overall low incompatible element abundances, the Sr concentration in the carbonatite and basanite samples range from 410–8,313 µg/g (average = 2,364 µg/g) except for NM23 from Agate Mountain with 15,647 µg/g of Sr, which is on the lower side of Sr concentrations found in carbonatites. Considering the extreme Sr isotope ratios of upper crustal material, the Sr isotope ratios of the carbonatite and basanite samples, however, are still sensitive to crustal contamination, especially in the silicious carbonatites with relatively low Sr concentration. As shown in Figure 6b, calcio-carbonatites from Agate mountain show a crude positive correlation of 1/Sr versus $^{87}Sr/^{86}Sr$, consistent with greater upper crustal contamination in samples with lower Sr concentration. If we assume that the source of the Agate Mountain HIMU rocks had an isotopic composition similar to St. Helena lavas (with $^{87}Sr/^{86}Sr$ of 0.7028), which were erupted on oceanic lithosphere, and average carbonatitic Sr concentration of 2742 ppm, the trend towards radiogenic Sr isotope compositions of the Agate Mountain carbonatites can be modelled by up to ~32% assimilation of regional upper crust (with an average $^{87}Sr/^{86}Sr$ of 0.77 and Sr concentration of 120 ppm) (Figure 6a). Alternatively, the high Sr isotope ratios could reflect a source feature (e.g. recycled marine carbonates), but this is not supported by the generally low $\delta^{13}C$ values of the Agate Mountain rocks (Figure 5), since marine carbonates generally have high $\delta^{13}C$ and $\delta^{18}O$ values and the Agate Mountain rocks only have high $\delta^{18}O$. Low-T alteration of recycled carbonated ocean crust, however, could have caused an increase in $\delta^{18}O$ but not of $\delta^{13}C$. In contrast, the two samples from Swakopmund (NM2018A) and Dicker Willem (NMH1) with slightly elevated $^{87}Sr/^{86}Sr$ ratios of 0.7038 require less than 8% assimilation of average crust.

In contrast to Sr, the Nd (79.7–1,675 µg/g) and Pb (2.85–1,108 µg/g) contents of the investigated samples (excluding secondary silicate rocks/carbonates and a Gross Brukkaros rhyolite) are generally much higher than in the regional upper crust i.e. the Nama group and Kuiseb, Khan, Etusis metasedimentary rock formations (average concentration of Nd is 37.0 and Pb is 18.0 µg/g; McDermott and Hawkesworth, 1990). Thus, these elements, and also their respective isotope ratios, are less susceptible to crustal contamination. Accordingly, our samples show very little variation in Nd isotopes (Figure 6a): Agate Mountain carbonatites range from 0.51271–0.51276 and silicate rocks from 0.51268–0.51278 (including NM31 and NM32 phonolite samples from Homrighausen et al., 2020), Dicker Willem from 0.51262–0.51269 and Swakopmund basanites from 0.51277–0.51282.

As noted above, however, all Dicker Willem samples have slightly less radiogenic Nd isotope ratios than St. Helena, which has a range of 0.51273 to 0.51287. The deviation of Dicker Willem sample NMH1 with a Nd isotope ratio of 0.51262 (and elevated Sr isotope ratio) can be explained by less than 10% crustal assimilation (Figure 7c). The remaining Dicker Willem samples also have slightly more radiogenic Sr and less radiogenic Nd isotope ratios and extend to more radiogenic Pb isotopic composition than the oceanic St. Helena basanites. Although the high-Ti Etendeka basalts (Gough-type EM1) have more radiogenic Sr and less radiogenic Nd than the Dicker Willem samples, they also have less radiogenic Pb isotope ratios and thus the Dicker Willem samples cannot be derived by mixing of St. Helena and high-Ti Etendeka type sources. We also note that no high-Ti basalts have been found in the Dicker Willem area to date. Finally, the two samples with the highest $^{206}Pb/^{204}Pb$ of 21.10 (NMH2) and 21.66 (NMH4) have O and C isotopic composition within the range of oceanic basalts and primary carbonatites. Therefore, the more radiogenic Sr and Pb but less radiogenic Nd isotope ratios than St. Helena (Figure 6a, 7) and the similar $^{206}Pb/^{204}Pb$ and $^{208}Pb/^{204}Pb$

but higher $^{207}Pb/^{204}Pb$ and $^{87}Sr/^{86}Sr$ and lower $^{143}Nd/^{144}Nd$ than Mangaia appears to be an inherent feature of Dicker Willem carbonatites rather than the result of crustal contamination.

5.2. Primary carbonatite melts and melt differentiation

Carbonatitic melts can be generated by (1) primary mantle melting, (2) liquid immiscibility and (3) fractional crystallization. Primary carbonatitic melts can be formed by partial melting of perovskite at transition zone depth, but the postulated primary carbonatite melts do not show negative anomalies for Hf and Zr (Figure 4a and Walter et al., 2008). The depletion of Hf and Zr, however, is a common feature of most carbonatites (e.g. Hoernle et al., 2002), including our samples. The HFSEs are highly compatible in certain minerals such as perovskite and rutile in eclogite (Walter et al., 2008 and references therein) during partial melting or crystal fractionation processes, thereby largely retaining these elements in the source as long as these phases are residual. Conversely, these elements are depleted in the magma. In addition, the immiscibility of silicate (e.g. phonolite) and carbonate melts could further enhance the depletion of HFSEs in carbonatites. We note that phonolites occur together with the carbonatites at Agate Mountain and Dicker Willem, consistent with a close relationship between these silicate and carbonate melts. Consequently, we assume that carbonatites are formed by low-degrees of melting of subducted, carbonated oceanic crust (returned to the surface by upwelling mantle plumes), coexisting with perovskite and majorite garnet in the deep upper mantle (Walter et al., 2008), and subsequently undergo an immiscible process at shallower depth. Following this model, the decoupling of carbon isotopes (more or less oceanic basalt values) and oxygen isotopes (distinctly elevated, Figure 4) could also reflect a source signal (recycled low-T altered ocean crust) rather than post-eruptive low-temperature alteration of the carbonatites.

In order to test the origin of carbonatite melts using their major and trace elements, we modelled the element concentrations generated from partial melting of eclogite (recycled ocean crust) coexisting with perovskite and majorite garnet, using the partition coefficients for these minerals determined from diamond inclusions (Walter et al., 2008). The compositions of primary carbonatite melts were calculated using the relationship $C_{melt} = C_{solid}/D$, where the coexisting mineral composition (C_{solid}) and the solid/melt partition coefficient (D) are reported in Appendix B. Then we modelled immiscibility of carbonatite from the silicate (phonolitic) melts, which we call "separated carbonatite magma" (Appendix B). Their compositions are calculated by relation $C_{separated\ carbonatite\ melt} = C_{primary\ carbonatite\ melt} \times D$, where the primary carbonatite melt concentrations are calculated above and the carbonatitic/phonolitic bulk immiscibility coefficients are listed in Appendix B (from Martin et al., 2013). The modelling results in a range of compositions because of different coexisting minerals, mineral/melt partition coefficients and carbonatite/silicate partition coefficients. The highest and lowest modelled values are plotted on Figure 4a, spanning the grey field called "calculated composition". Ta, K, P and Ti concentrations are not modelled because of the lack of data from the mineral inclusions and partition coefficients for these elements.

Our calculated carbonatite compositions largely overlap with the Agate Mountain and Dicker Willem patterns including their distinctive Zr and Hf depletion. The variation in Pb concentration in the analyzed lavas could be explained by some crustal assimilation. The greater depletion of Hf and Zr shown by some of the lavas may be caused by enhanced fractional crystallization of e.g., zircon, garnet and/or titanite. Our results are therefore consistent with the hypothesis that calcio-carbonatites are created by low-degree melts of recycled, carbonated ocean crust (Dasgupta et al., 2007; Hoernle et al., 2002) with carbonatitic melts, being subsequently separated from silicate

(phonolitic) melts by immiscibility. We note that magnesio-carbonatites show larger range of LREE (e.g. La and Ce, Figure 4) and possess more depleted Hf and Zr than the modelled composition.

5.3. Lithospheric versus asthenospheric origin

There are two main hypothesis concerning the sources of carbonatites. They can be derived from (1) mantle plume-metasomatized subcontinental lithospheric mantle - SCLM (Le Roex and Lanyon, 1998), or (2) deep-seated mantle plumes (e.g. Ernst and Bell, 2010; Hoernle et al., 2002).

Low-degree melts of SCLM metasomatized by Tristan-Gough plume head melts can explain the EM1-like composition of Cretaceous carbonatites in the Damara Belt that have ages of 130–120 Ma (Le Roex and Lanyon, 1998; Zhou et al., 2022). No evidence, however, has been found to date that the SCLM in NW Namibia has a composition similar to that of the significantly younger (~84–49 Ma) HIMU-like carbonatites and alkaline rocks considered here. If the SCLM was metasomatized by the Tristan-Gough plume, and played an important role in generating the Agate Mountain, Swakopmund and Dicker Willem magmas, we would expect them to have a similar isotopic composition to the Etendeka flood basalts, rather than HIMU-type compositions. Furthermore, the mantle (peridotite) xenoliths found in the Swakopmund plug magmas and at other locations in Namibia, e.g. at Okenyenya, an alkaline intrusive complex located ~200 km NE of Swakopmund which formed shortly after the Etendeka event between ~129 and 123 Ma (Milner et al., 1993), do not have a HIMU-like composition (Figure 6). Therefore, there does not appear to be a widespread distribution of HIMU material in the regional subcontinental lithosphere (Class and le Roex, 2006). In addition, xenoliths from the lower crust (also found at Okenyenya) that are proposed to have been affected by metasomatism of the Tristan-Gough plume do not have HIMU-type compositions either (Figure 6) (le Roex and Class, 2014). Instead, the Okenyenya lamprophyre lavas, believed to be derived from

metasomatized lithospheric mantle (Le Roex and Lanyon, 1998), have an EM1-like (depleted Etendeka type) composition with high $^{207}Pb/^{204}Pb$ and low $^{208}Pb/^{204}Pb$ for a given $^{206}Pb/^{204}Pb$ (Figure 7). Furthermore, the postulated trace element enrichment in the lithosphere by this metasomatism (if directly related to the Etendeka flood basalt event as generally believed, e.g., Le Roex and Lanyon, 1998) occurred just ~50–85 Ma before the emplacement of the post-Etendeka carbonatites and silica-undersaturated volcanism investigated here. Therefore, the time interval is not long enough to generate HIMU compositions in the magma source by radiogenic ingrowth (1.0–3.2 Ga; Homrighausen et al., 2018b). The Damara Mobile Belt, primarily underlying the study area, was formed within the last ~660 Ma (e.g. Nascimento et al. 2017) and thus also appears too young to generate HIMU-type lavas. Recently, Mazza et al. (2019) published isotope data for Bermuda lavas, which extend to very high $^{206}Pb/^{204}Pb$ (almost to 22.0). They are fundamentally different from classical HIMU-type rocks from St. Helena and Mangaia and from the carbonatites and undersaturated rocks studied here because they have much lower $^{207}Pb/^{204}Pb$ for any given $^{206}Pb/^{204}Pb$ (figure 7a). Mazza et al. (2019) proposed that the high $^{206}Pb/^{204}Pb$ but low $^{207}Pb/^{204}Pb$ isotope ratios in Bermuda lavas formed by radiogenic ingrowth of Pb within a relatively short time interval (<650 m.y.), as a result of storage of young slabs subducted during the formation of Pangea in the mantle transition zone. Due to the much shorter half-life of ^{235}U (decaying to ^{207}Pb) compared to ^{238}U (decaying to ^{206}Pb), there is no longer much ^{235}U left on Earth. The high ^{207}Pb found in classical HIMU requires a high μ early in Earth's history (>1 Ga, e.g. Homrighausen et al., 2018b). Although rafts of Paleoproterozoic Congo or Kalahari Craton may have been stranded in the lower parts of the Damara Mobile Belt, it is unlikely that Paleoproterozoic SCLM survived formation of the mobile belt and the younger Parana-Etendeka flood basalt event. Since a lithospheric origin for these

carbonatites / silica-undersaturated rocks is highly unlikely, these rocks most likely represent primary melts from an upwelling deep-seated mantle plume having a HIMU-type composition, such as proposed for the Canary and Cape Verde carbonatite complexes (e.g., Hoernle et al., 2002). Below we will show seismic evidence that mantle is still upwelling from the base of the lower mantle, supporting a sublithospheric origin for the source material of the ≤84 Ma year HIMU-type volcanism along the western African margin.

5.4. Isotopic constraints of post-Etendeka HIMU volcanism

As mentioned above, the post-Etendeka HIMU volcanism along the coast of Namibia (Agate Mountain, Dicker Willem and basanite plugs near Swakopmund) are significantly younger than the EM1 dominated Etendeka flood basalt event. The temporal relationship and isotopic composition of these carbonatitic and silica-undersaturated igneous rocks are very similar to the late-stage HIMU volcanism on the Walvis Ridge and Shona tracks, which succeeded the formation of the age-progressive volcanism of the EM1-dominated Tristan-Gough-Walvis and Shona hotspot tracks by ~30 Ma at a given location (Homrighausen et al., 2018a; Homrighausen et al., 2020). It is likely that the carbonatitic complexes and basanitic plugs were derived from the same source as the late-stage HIMU volcanism on the Walvis Ridge and may also form one or several age-progressive hotspot track(s) extending into Angola (Homrighausen et al., 2020) and South Africa, respectively. Therefore, we will compare the composition of the carbonatite / silica-undersaturated rocks with the late-stage Walvis Ridge seamounts and St. Helena in more detail below.

Except for their Sr isotope ratios (Figure 6), which extend to much higher ratios than St. Helena HIMU and which are most likely caused by the susceptibility of Sr to crustal contamination of these relatively Sr-poor carbonatite magmas (see Section 5.1), all other isotope ratios of the carbonatites

analyzed in this study (Figure 6, 7) are similar to the HIMU-type late-stage seamounts. These include the late-stage seamounts on and next to the Walvis Ridge and Shona volcanic track (Walvis-Mocamedes and Richardson-South Africa; Homrighausen et al., 2020), whose composition was proposed to be generated by mixing of a HIMU endmember with a low-μ component (a mixture of Gough-type plume and normal depleted upper mantle; Homrighausen et al., 2018a). Likewise, the lavas investigated here converge towards extreme HIMU-type endmembers, regardless if the depleted end of possible mixing trajectories point to depleted upper mantle, Etendeka-type end members, or local crust (Figures 6, 7).

Compared to the silicate HIMU-like late-stage volcanism on Walvis Ridge (yellow field in Figure 7), the carbonatites of this study show slightly more radiogenic Pb and less radiogenic Nd isotope ratios. The two Dicker Willem samples (NMH2 and NMH4) with mantle-type O and C isotopic composition also have the most radiogenic Pb and the least radiogenic Nd (excluding sample NMH1 which shows evidence of crustal contamination). NMH2 and NMH4 also have slightly higher initial $^{206}Pb/^{204}Pb$ than the field of the classic St. Helena HIMU endmember calculated at 70 Ma. A similar deviation of $^{206}Pb/^{204}Pb$ has also been observed in previously published data from East African carbonatites (Bell and Tilton, 2001). Therefore, the most extreme (with most radiogenic $^{206}Pb/^{204}Pb$) HIMU signal may be most pronounced in very low-degree carbonatitic melts (in comparison to the basanitic melts exposed on St. Helena Island or on the Walvis and Shona hotspot tracks). We note that the Pacific HIMU endmember locality Mangaia Island, Austral volcanic chain (Nakamura and Tatsumoto, 1988; Woodhead, 1996) also has more radiogenic $^{206}Pb/^{204}Pb$ than St. Helena lavas (Chaffey et al., 1989). The Dicker Willem NMH2 and NMH4 samples, however, have slightly higher $^{207}Pb/^{204}Pb$ and $^{87}Sr/^{86}Sr$ and lower $^{143}Nd/^{144}Nd$ ratios than lavas from Mangaia Island, Austral island chain. In conclusion, the

Dicker Willem carbonatities appear to represent one of the most extreme HIMU-type magmas found on Earth thus far, defining a third HIMU-type end member, in addition to St. Helena and Mangaia/Tubuaii ocean islands.

One could argue that the slightly lower Nd and elevated Sr (if alteration is neglected) isotopic ratios of the carbonatites are more FOZO-like than St. Helena-like, as FOZO is quite compositionally heterogeneous or has a range of values (e.g. $^{206}Pb/^{204}Pb$= 18.5 to 20.5), and is interpreted to reflect comparatively young HIMU (e.g., Stracke et al., 2005). According to the preceding EM-1 (Etendeka) plume head event could have metasomatized FOZO-like material within the shallow upper mantle beneath southern Africa, which later produced low-degree carbonatitic melts (as proposed for the East African Rift System, e.g. Castillo et al., 2020). The time delay in the generation of these carbonatitic melts could have generated the very radiogenic Pb isotopes (exceeding those of St. Helena) in the source as a result of radiogenic ingrowth, since samples with the most radiogenic Pb also have the highest U/Pb ratios (Appendix A). The ~50 m.y. between the emplacement of the Etendeka plume head and the formation of the carbonatitic melts, however, is not sufficient to generate such an extreme HIMU composition beneath southern Africa by radiogenic ingrowth alone (see above). An unrealistically high μ value of >500 would be required to produce $^{206}Pb/^{204}Pb$ ratio of >21.0 from an EM1-like source (such as NAM21 with $^{206}Pb/^{204}Pb$=17.11) and this would only elevate the $^{207}Pb/^{204}Pb$ ratio to 15.67 (significantly lower than observed in the Namibian HIMU carbonatites). A value of >500 is also considerably higher than the μ's found in the two Dicker Willem samples with mantle-like O and C isotopes and with the highest $^{238}U/^{204}Pb$ ratios (67–92). Furthermore, thorogenic Pb isotope composition ($^{208}Pb/^{204}Pb$ lower than Mangaia and overlapping with St. Helena) does not support such a process either. In addition, the Swakopmund basanites, for

which Hf isotope ratios could be generated ($^{176}Hf/^{177}Hf_{70\ Ma}$=0.282862-0.282894), show values similar to St. Helena HIMU (0.282830-0.282853, which is significantly lower than FOZO = 0.28294-0.28304; Stracke et al., 2005). Finally, as already mentioned above (Section 5.3.), none of the analyzed regional SCLM xenoliths show HIMU-like signatures.

In conclusion, carbonatites and silica-undersaturated rocks from Agate Mountain, Swakopmund, Dicker Willem, the Walvis–Mocamedes and Richardson–South Africa tracks appear to be derived from a HIMU-type mantle source, similar to the St. Helena source, although the Dicker Willem carbonatites may indicate a new HIMU-type flavor, similar but not identical to the Mangaia source.

5.5. Belt of HIMU volcanism along the SW coast of Africa

The Agate Mountain carbonatites and associated phonolites, dated at 83–82 Ma (Homrighausen et al., 2020), have nearly completely overlapping isotopic composition, consistent with derivation from a common source at a similar time as implied by field studies (Miller, 2008). Although early (~132 Ma) tholeiitic magmatism in southern Angola can be associated with the EMI (Gough) type Etendeka flood basalts, late-stage alkaline basalts have ages of 93–85 Ma and HIMU-type composition ($^{87}Sr/^{86}Sr_{70\ Ma}$ = 0.70277 to 0.70303 and $^{143}Nd/^{144}Nd_{70\ Ma}$ = 0.51276; Campeny et al., 2015; Strganac et al., 2014 and references therein). Therefore, the Agate Mountain carbonatite complex appears to be part of a continuous Walvis Ridge–Mocamedes HIMU hotspot track (Figure 1) in accordance with the NW-directed African plate movement (Homrighausen et al., 2020).

The Dicker Willem carbonatites also appear to be aligned in an age-progressive succession of adjacent HIMU volcanism extending in the direction of plate motion. This track comprises (from NE to SW) Gibeon Kimberlites (79–72 Ma) and Gross Brukkaros (77±2 Ma), Dicker Willem carbonatites

(49±1 Ma), Klinghardt phonolites (46 Ma), Swartkop phonolite (37 Ma; abbreviated as SK in Figure 1) and the Schwarzeberg nephelinite (36 Ma; abbreviated as SB in Figure 1) all emplaced on continental crust (Marsh et al., 2018; Reid et al., 1990 and references therein) and the Vema seamount (15 Ma; O'Connor and le Roex, 1992). The Gibeon Kimberlites have similar isotope ratios to Walvis–Mocamedes and Richardson–South Africa lavas (Figure 7), further supporting the idea of a common deep HIMU source (Section 5.4) feeding separate hotspot tracks on the surface. A rhyolite from Gross Brukkaros also shows HIMU-like Pb isotope ratios (Figure 7c, d), although its elevated Pb concentration (Figure 4c), radiogenic $^{87}Sr/^{86}Sr$ and unradiogenic $^{143}Nd/^{144}Nd$ indicate significant crustal contamination. Schwarzeberg nephelinites also have HIMU-like Sr-Nd-Pb isotopic composition (Janney, 2007).

There is also a group of low-volume, silica-undersaturated volcanic rocks and carbonatites of HIMU composition located near the southwest African coast between the potential Vema and Shona tracks, consisting of the Warmbad, Bushmanland and Namaqualand volcanic clusters (abbreviated as WBN in Figure 1). These volcanic complexes, located 500 km north of the axis of the Shona hotspot track, show a plausible age progression (83–38 Ma) similar to the Shona track (Figure 1).

The Swakopmund basanites cannot be associated with any nearby age-progressive volcanism, yet they show the same isotopic composition as other HIMU-like post Etendeka carbonatites and silica-undersaturated volcanism. They almost completely overlap with the late-stage Walvis Ridge seamounts (likewise basanites and alkali basalts) in all isotopic systems, suggesting that they are derived from a similar source.

All of the younger age-progressive hotspot tracks (St. Helena, Walvis–Agate Mountain–Mocamedes, Gibeon–Dicker Willem–Vema, Warmbad–Bushmanland–Namaqualand and Richardson–South Africa), which become younger to the SW, have HIMU-type isotopic composition, which is distinct from the older EM1-type hotspot tracks (Tristan-Gough, Discovery and Shona) and associated flood basalts (Karoo, Parana-Etendeka) and the ambient depleted upper mantle (DMM). As illustrated in Figure 8, the EM and HIMU-type hotspot tracks have distinct compositions from each other and from depleted Atlantic N-MORB-type upper mantle. We thus propose that there is a belt of HIMU rocks that extends from St. Helena Island in the Central South Atlantic to Angola, along the western coast of Namibia to the southern tip of South Africa. This HIMU volcanic belt extends sub-parallel to the southwestern African LLSVP margin but is located 900–1200 km within the LLSVP (blue stippled line shows location of upward step in the LLSVP in Figure 1).

A N-S profile from seismic tomography model SEMUCB-WM1 (French and Romanowicz, 2014) through the EM1-type Tristan-Gough, Discovery and Shona hotspots shows a large low-velocity anomaly (~1600–1800 km width in the N-S direction) ascending from the southwestern (outer) margin of the African LLSVP to a depth of ~1100 km (Figure 9a). Between depths of ~2000–1000 km, three arms/branches emanate from this large (trunk-like) anomaly and extend upwards beneath the SW ends of the Tristan-Gough, Discovery and Shona hotspots. Therefore, the three hotspots with a common Gough-type EMI composition appear to be derived from a single superplume type upwelling from the southwest boundary of the African LLSVP. The outer margin of the LLSVP has been proposed to be the generation zone for (large) primary mantle plumes (e.g., Burke et al., 2008). Since the current location of the EM1 hotspots in the South Atlantic (Tristan-Gough, Discovery and Shona) and the reconstructed locations of their corresponding flood basalt (plume head) stages

(Etendeka and Karoo) lie above this boundary, it is likely that the EM1 source resides in this part (or in the proposed lower "primordial" layer; e.g. Ballmer et al., 2016) of the LLSVP.

The seismic tomographic models further show a steep inner step/slope on the surface of the African LLSVP about 900–1200 km eastward from its southwest margin (e.g., French and Romanowicz, 2014) (Figure 9b). Seismic low-velocity anomalies beneath the belt of HIMU volcanism can be traced into the lower mantle to the upper portion of the step/slope in the LLSVP (Figure 9b, c). Additionally, as shown in Figure 1 by the blue stippled belts, the strike of this step, if projected to the surface, roughly connects the projected present location of the different age-progressive trends (blue circles in Figure 1) of HIMU volcanism (formed between ~120–15 Ma). Therefore, it appears that the southwestern portion of the African LLSVP has at least two distinct compositional domains. The change from EMI-type compositions at the southwest margin of the LLSVP to HIMU-type compositions could either reflect lateral and/or vertical chemical zonation of the African LLSVP. Based on various geophysical observations, Ballmer et al. (2016) proposed a layered LLSVP with a lower "primordial" layer, which possibly may reflect the source of the EMI-type primary hotspots, and an upper "ancient basaltic" layer, which could represent the source of the secondary HIMU-type hotspots. Voluminous (plume head) and subsequent continuous (plume tail) drainage along the outer margins of the LLSVP (Etendeka/EM1) might cause destabilization of internal portions of the LLSVP, which could become secondary plume generation zones taping a different geochemical reservoir(s), e.g. HIMU-type. Because these secondary hotspots form on the same moving plate as the primary hotspots, their (HIMU) volcanism overlies the older (EM 1) volcanism, while displaying a similar age progression.

6. Conclusions

The Agate Mountain calcio- to magnesio-carbonatites show extreme enrichment in REE and Ba, Th and U, but relative HFSE depletion. Most samples have mantle-like $\delta^{13}C$ but elevated $\delta^{18}O$, most likely reflecting low-temperature alteration. The carbonatites also have HIMU-like Sr-Nd-Pb isotopic composition, similar to mafic silicate-undersaturated rocks of the Walvis-Mocamedes volcanic track and related phonolites (83–82 Ma). Therefore, we conclude that the Agate Mountain carbonatite complex also forms part of the Walvis-Mocamedes HIMU volcanic track.

The Swakopmund basanites and Dicker Willem calcio-carbonatites, located near the Atlantic coast of southwestern Namibia, also show enrichment of incompatible elements. Although there is considerable variation in O and C isotope ratios, two samples have mantle-like ratios. These carbonatites also have HIMU-like Sr-Nd-Pb isotopic composition, although the two samples with mantle-like O and C isotopes have more radiogenic $^{206}Pb/^{204}Pb$ ratios than St. Helena rocks. The $^{206}Pb/^{204}Pb$ and $^{208}Pb/^{204}Pb$ ratios are similar to Mangaia volcanic rocks, but the $^{207}Pb/^{204}Pb$ and $^{87}Sr/^{86}Sr$ are higher and $^{143}Nd/^{144}Nd$ lower, identifying a unique endmember HIMU flavor in addition to St. Helena and Mangaia/Tubuaii ocean islands. Even though the Swakopmund basanites are not part of an age-progressive track and the nearby Gibeon–Dicker Willem–Vema track show a compressed age-progression, they appear to be derived from a similar HIMU source, as proposed for the St. Helena, Walvis–Mocamedes and Richardson–South Africa age-progressive volcanic tracks, and could be derived from weak pulsating plumes or ascending blobs.

Together with other clusters of HIMU volcanism, such as Warmbad – Bushmanland - Namaqualand and Richardson – South Africa track volcanism along the SW coast of South Africa, the HIMU volcanism forms a belt running sub-parallel to the outer LLSVP margin. Combining the geochemical

data with seismic tomography, it is proposed that EMI-type plumes (Tristan-Gough, Discovery and Shona) ascend from the outer margin of the LLSVP. Seismic tomography data suggest that the low-velocity roots of these hotspots are connected at mid mantle depths to a dome-like upwelling from the base of the lower mantle. Derivation from a common low-velocity anomaly is consistent with the uniform Gough-type EMI composition of these three plumes pointing towards derivation from a common source. In contrast, the HIMU volcanism appears to be related to a topographic step on the surface of the LLSVP, about 900–1200 km east of the outer margin and therefore within the LLSVP. Multiple upwellings along this step appear to have fed the widespread belt of HIMU volcanism extending from St. Helena along the southwest coast of Africa (Angola, Namibia and South Africa) to the southern tip of South Africa. Except for St. Helena and possibly Vema, the secondary HIMU hotspots appear to have ceased activity, since no young HIMU volcanism has been found on the seafloor at the ends of these tracks thus far.

Acknowledgements

We thank K. Junge, S. Heun, and U. Westernströer for analytical support; the Geological Survey of Namibia for giving permission to carry out field studies and clearance for sending samples out of Namibia for geochemical analyses; and the German Ministry of Education and Research (BMBF; project SO233-Walvis II; grant number: 03G0233A) for support for a field campaign after the SO233 cruise and analytical support. HZ's doctoral position was funded by the China Scholarship Council (CSC). Additional funding for the project came from the GEOMAR Helmholtz Centre for Ocean Research Kiel. Reviews by P. Castillo, C. Chauvel and an anonymous reviewer helped improve the manuscript; X.-H. Li and G. Shellnutt are thanked for editorial handling of the manuscript.

Figures

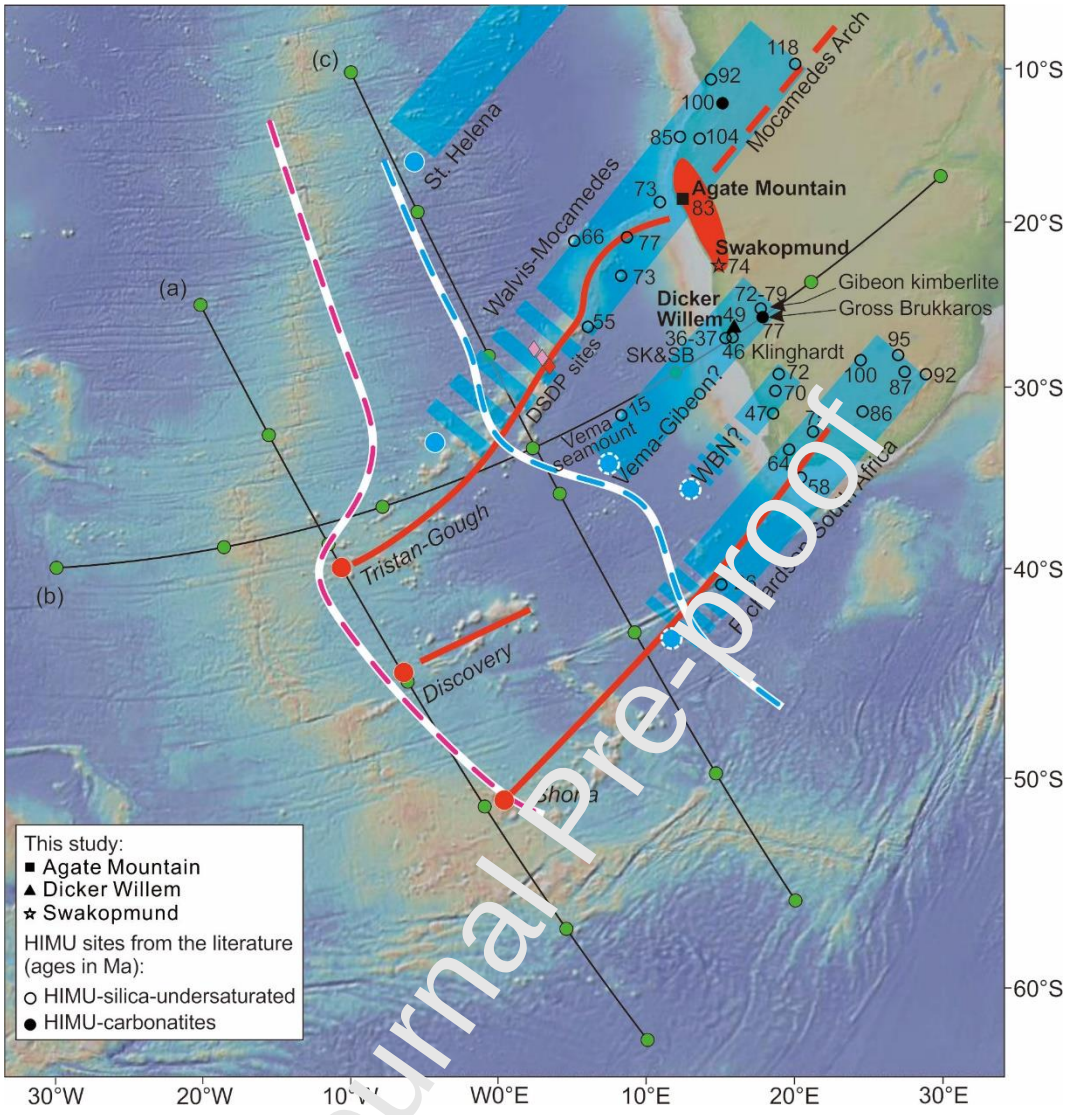

Figure 1: Map of the South Atlantic and southwest Africa, showing all previously known sample locations with HIMU signature in this area (circles) and the average ages of each sample site (numbers in Ma) (Homrighausen et al., 2020; Marsh et al., 2018; Reid et al., 1990 and references therein). Filled symbols indicate carbonatites and open symbols denote silica-undersaturated rocks. Red field adjacent to the intersection of Walvis Ridge with the African continent denotes the location of Etendeka flood basalt volcanism (Marsh et al., 2001). Hotspot tracks with EMI-type composition are shown in red and those with HIMU-type

compositions with thick blue belts. The red and blue circles are the possible present positions of the EM1 and HIMU hotspot tracks, respectively. Thick red/white and blue/white dashed lines mark the postulated boundaries of the EMI and HIMU compositional domains, respectively, in/on the large low-shear velocity province (LLSVP) at the base of the lower mantle (projected to the surface) – see section 5. Thin black lines (a, b, c) connecting green circles denote the seismic tomography profile locations of Figure 9a, b and c. WBN represents the Warmbad, Bushmanland and Namaqualand volcanic clusters. Map generated by GeoMapApp (http://www.geomapapp.org).

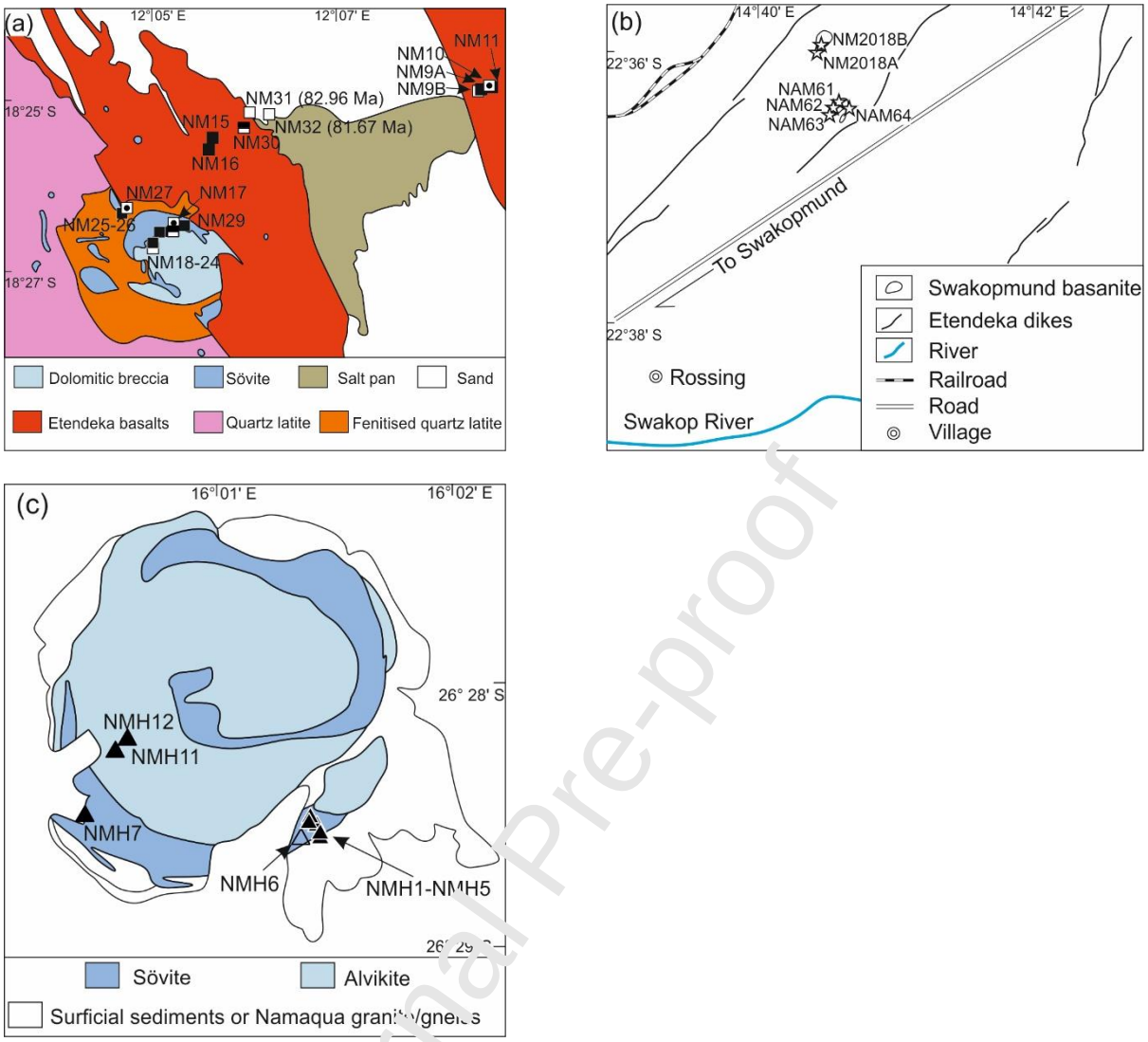

Figure 2: Simplified geological/topographic maps of (a) Agate Mountain after Miller (2000), (b) Swakopmund basanite outcrops, and (c) Dicker Willem complex after Cooper (1988). Filled / open sample symbols denote carbonatites / silica-undersaturated rocks, respectively. The open symbols with a dot in the center denote secondary silicate and carbonate veins.

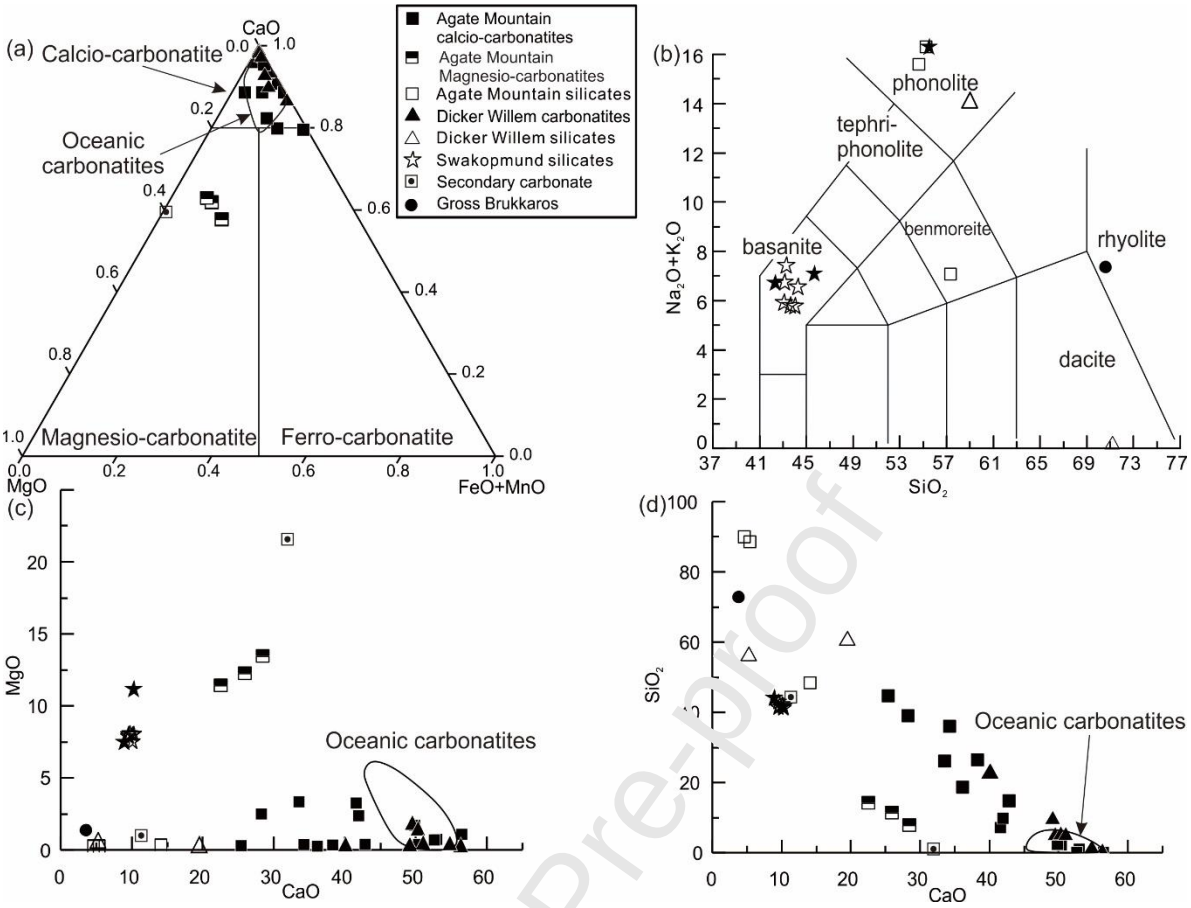

Figure 3: (a) Carbonatite classification diagram after Le Bas and Streckeisen (1991). Most samples from Agate Mountain and Dicker Willem are calcio-carbonatites. Three samples from Agate Mountain are magnesio-carbonatites. (b) Sampled silicates of Agate Mountain (with two phonolites included from Homrighausen et al., 2020), Dicker Willem and the Swakopmund plugs (solid black stars denote data from Whitehead et al., 2002) plotted (as weight percentages recalculated to 100% on a volatile-free basis) on the total alkali vs. silica diagram (TAS) of Le Bas and Streckeisen (1991). (c) CaO vs MgO and (d) CaO vs SiO_2 (in wt.%). Oceanic carbonatite field shown for comparison (Hoernle et al., 2002).

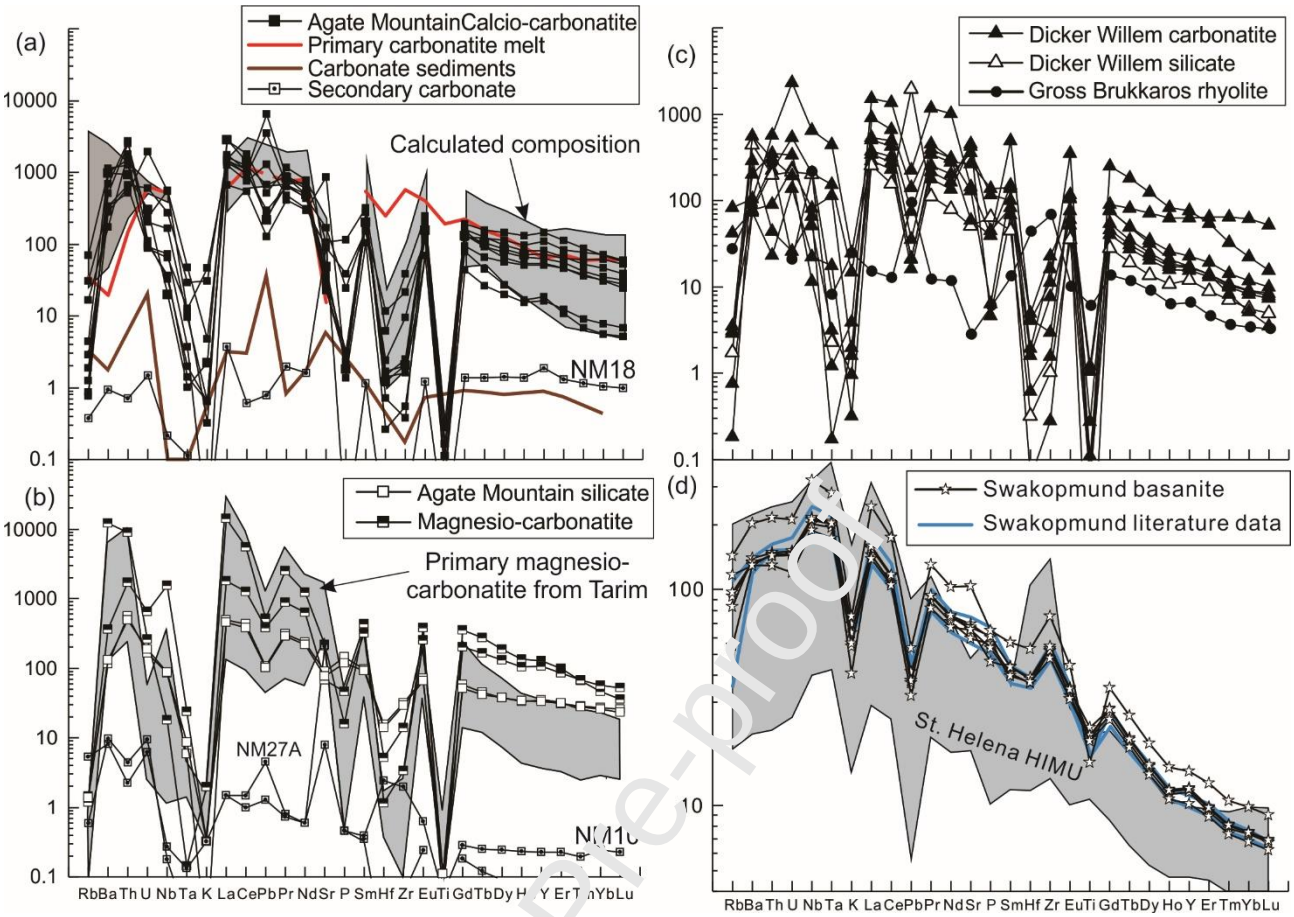

Figure 4: Multi-element diagrams normalized to primitive mantle (Sun and McDonough, 1989): (a) Calcio-carbonatites from Agate Mountain compared with estimated primary carbonatite melts (see section 5.2 and Table 1; Walter et al., 2008), calculated composition of carbonatite melts (grey field, see section 5.2 and Table 1 for details of calculation) and the average composition of carbonate sediments (Frimmel and Lane, 2005). (b) Magnesio-carbonatite and silicate-undersaturated rocks from Agate Mountain compared with the primary magnesio-carbonatites from the Tarim LIP (Cheng et al., 2017). (c) Carbonatite and silicate rocks from Dicker Willem and Gross Brukkaros. (d) Basanites from Swakopmund plugs (including two published Swakopmund basanites from Whitehead et al. (2002) compared with basanites from St. Helena with HIMU composition (Chaffey et al., 1989; Willbold and Stracke, 2006).

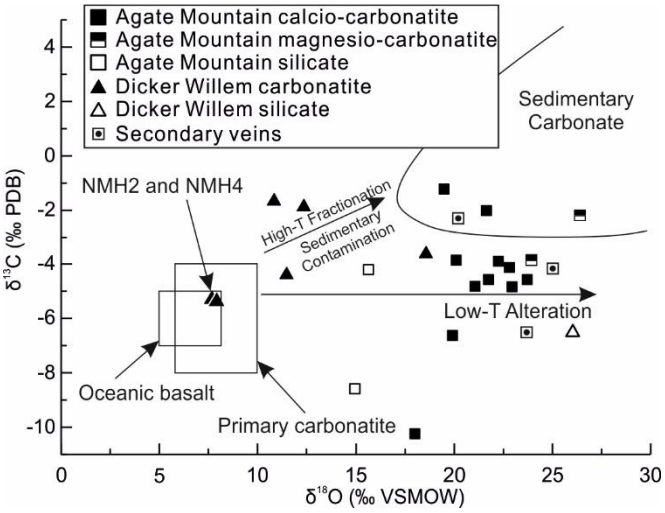

Figure 5: Oxygen and carbon isotopes of the investigated rocks from Agate Mountain and Dicker Willem. The composition of primary carbonatite and oceanic basalts are from Keller and Hoefs (1995). Most samples have higher $\delta^{18}O$ than primary carbonatite but similar $\delta^{13}C$, suggesting low temperature alteration (Hoefs, 2002).

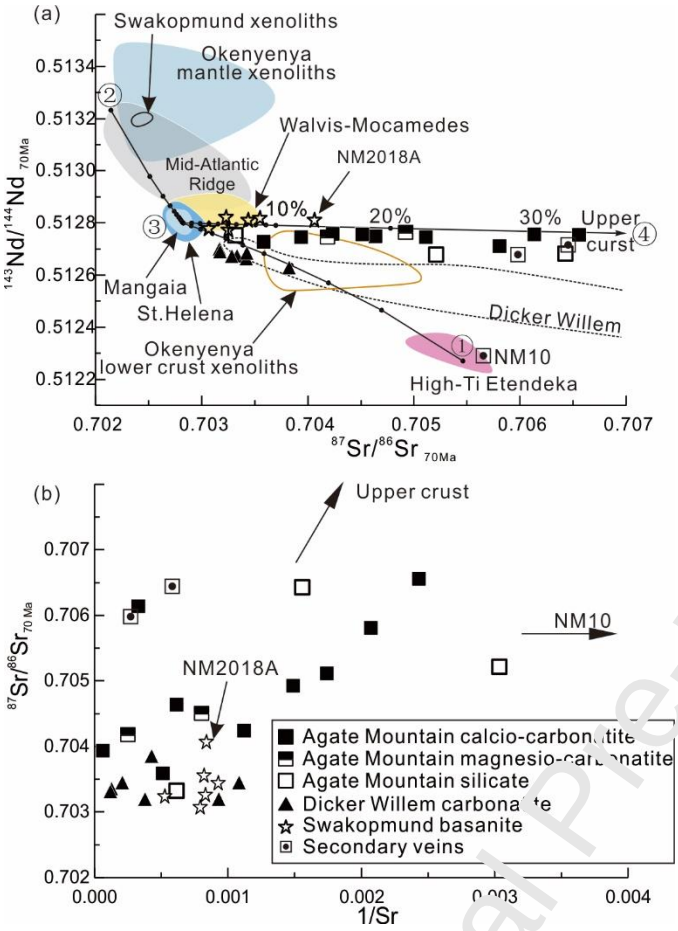

Figure 6: (a) $^{87}Sr/^{86}Sr$ vs $^{143}Nd/^{144}Nd$ ratios (at 70 Ma) of the investigated rocks showing possible mixing trends. The trend in the Agate Mountain samples towards extremely high $^{87}Sr/^{86}Sr$ isotope ratios is consistent with crustal assimilation (see Section 5.1 for detailed discussion). Bulk mixing lines are calculated for endmember compositions of ① Gough-type sample NAM21 from northern Etendeka high-Ti flood basalt (Zhou et al., 2020),② the most depleted sample from the Mid-Atlantic Ridge representing upper mantle (CHRRI88-016-101; Class and Lehnert, 2012), ③ St.Helena HIMU (Chaffey et al., 1989), and ④ an upper continental crustal component (average composition of the Nosib and Swakop metasedimentary group samples; McDermott and Hawkesworth, 1990). Black dots on the mixing lines mark 10% increments except when marked otherwise. For a better comparison

of the samples with different ages, i.e., to minimize the effect of variable time lengths for radiogenic ingrowth, all initial ratios are projected to an average age of 70 Ma by using the following assumed mantle source compositions according to their respective affiliation to the following reference fields: Gough EM1 composition: U/Pb = 0.1367, Th/Pb = 0.6758, Rb/Sr = 0.0204, Sm/Nd = 0.3378; HIMU-St. Helena: U/Pb = 0.3043, Th/Pb = 0.9565, Rb/Sr = 0.0071, Sm/Nd = 0.3590; Mid-Atlantic Ridge basalts: U/Pb = 0.1667, Th/Pb = 0.4444, Rb/Sr = 0.0065, Sm/Nd = 0.4114 (Homrighausen et al., 2018a; Zhou et al. 2020 and references therein). Reference sources: High-Ti basalts from Northern Etendeka (representing the Gough-type EM1 plume source in the study area) (Zhou et al. 2020); Mid-Atlantic Ridge (Class and Lehnert, 2012); Walvis–Mocamedes (HIMU-composition) hotspots (Homrighausen et al., 2018a; Homrighausen et al., 2018b); St. Helena HIMU (Chaffey et al., 1989; Willbold and Stracke, 2006); and published Dicker Willem data (Cooper and Reid, 2000; Cooper and Reid, 1998); Okenyenya mantle and lower crust xenoliths (Class and le Roex, 2006; le Roex and Class, 2014); Swakopmund xenoliths (Class and le Roex, 2006); Mangaia HIMU from Austral volcanic chain (Nakamura and Tatsumoto, 1988; Woodhead, 1996). (b) 1/Sr vs initial $^{87}Sr/^{86}Sr$. Arrows point in the direction of upper crustal contamination (Nosib and Swakop metasediments; McDermott and Hawkesworth, 1990) and towards sample NM10 composition, a secondary silicate vein with very low Sr concentration and with the same $^{87}Sr/^{86}Sr$ and $^{143}Nd/^{144}Nd$ as its hosting Etendeka (Gough-type) flood basalt.

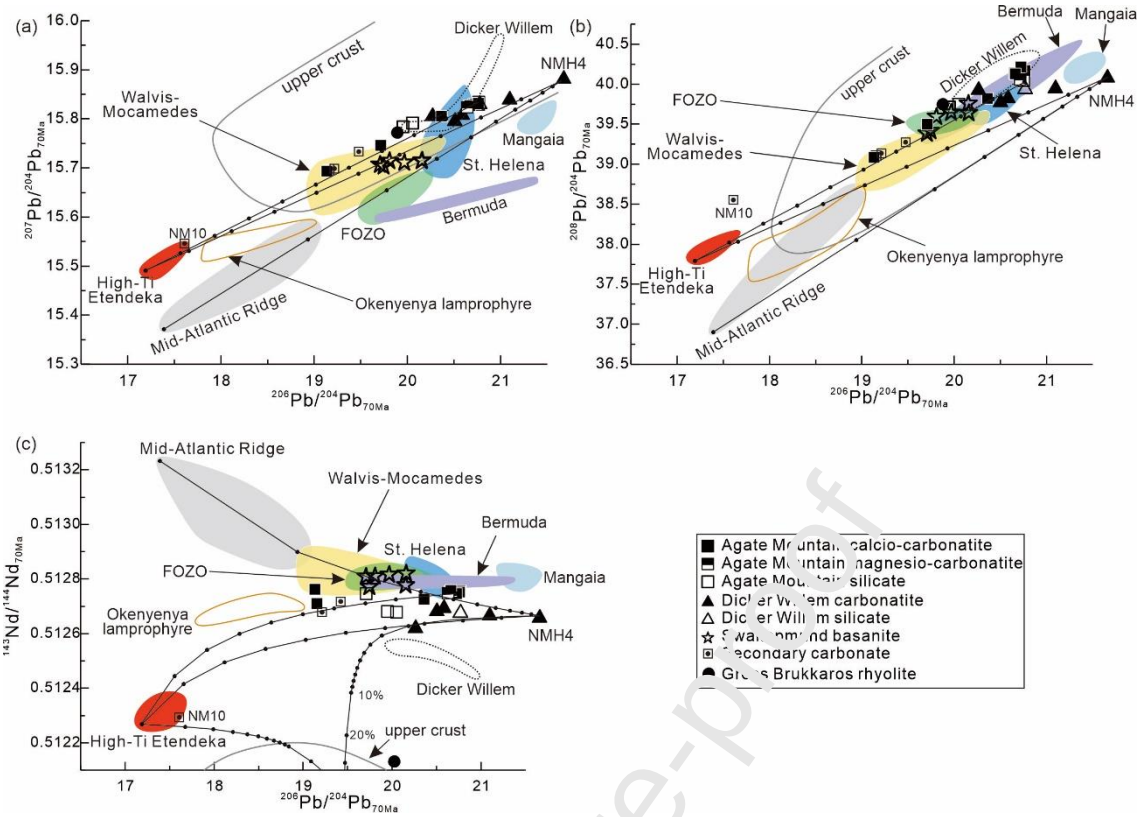

Figure 7: (a) $^{206}Pb/^{204}Pb$ vs. $^{207}Pb/^{204}Pb$, (b) $^{206}Pb/^{204}Pb$ vs. $^{208}Pb/^{204}Pb$ and (c) $^{206}Pb/^{204}Pb$ vs. $^{143}Nd/^{144}Nd$ isotope diagrams (at 70 Ma ago). Data sources and endmember compositions used for calculation of mixing lines and projection of reference field to 70 Ma are the same as in Figure 6, except for the additional mixing endmember of NMH4. Black dots on the mixing lines mark 10% increments except when marked. Reference sources: Okenyenya lamprophyre (Le Roex and Lanyon, 1998), Bermuda (Mazza et al., 2019) and FOZO (Stracke et al., 2005 and references therein).

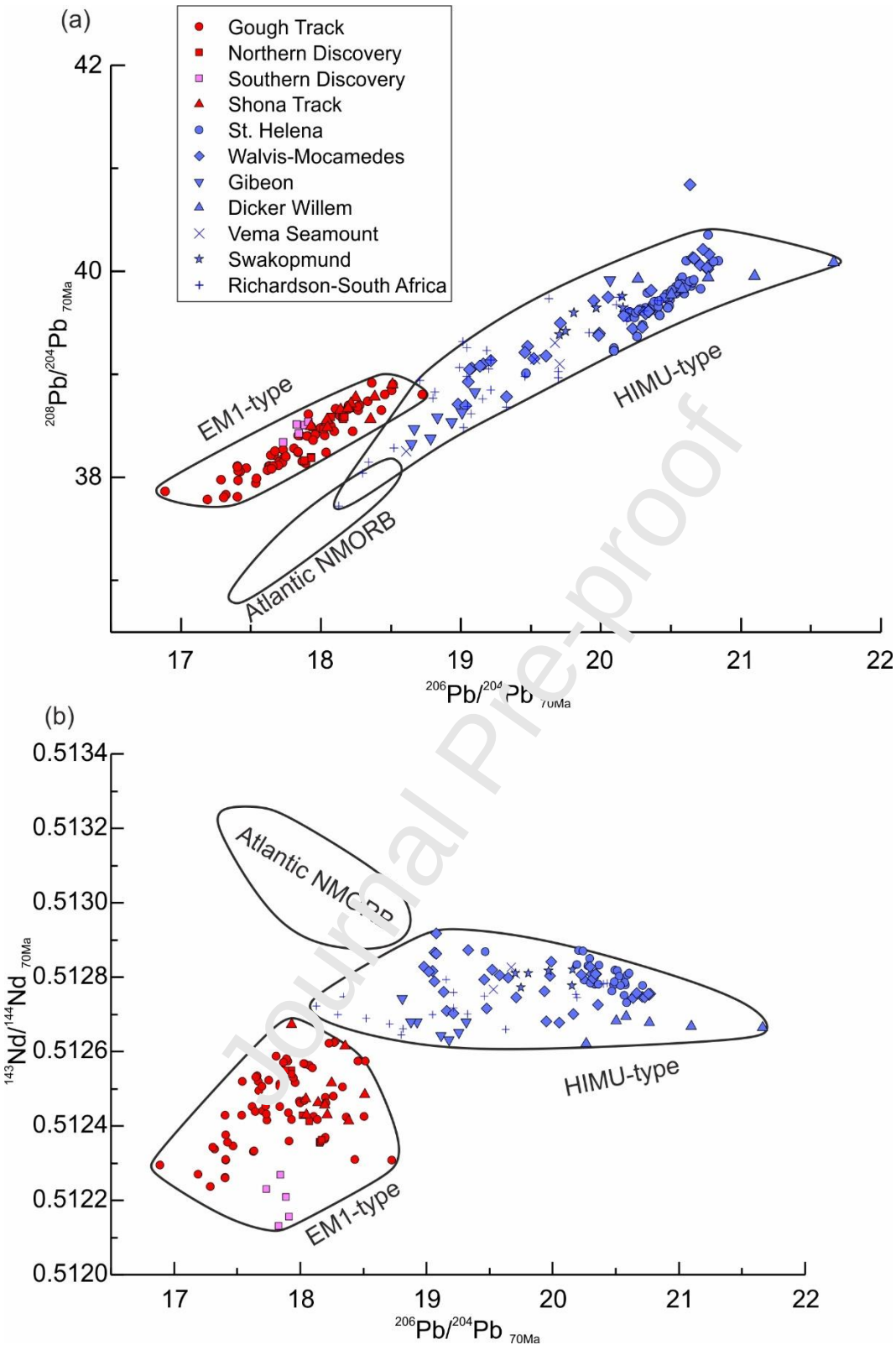

Figure 8: (a) $^{206}Pb/^{204}Pb$ vs. $^{208}Pb/^{204}Pb$ and (b) $^{206}Pb/^{204}Pb$ vs. $^{143}Nd/^{144}Nd$ isotope diagrams (projected to 70 Ma ago), showing distinct compositions for South Atlantic depleted upper

mantle, South Atlantic (EMI-type) mantle plumes and African margin (HIMU-type) mantle upwellings. South Atlantic depleted upper mantle is based on the composition of Mid-Atlantic Ridge (Atlantic NMORB) samples (Class and Lehnert, 2012), excluding samples located adjacent to Azores (35°N–43°N), Sierra Leone (1.5°S–6°N), Ascension (~9°S) and Jan Mayen (~71°N) plumes. The EM1-type field comprises samples from the Gough track (Hoernle et al., 2015; Homrighausen et al., 2019; Rohde et al., 2013), Northern and Southern Discovery (Schwindrofska et al., 2016), and Shona track (Hoernle et al., 2016). The HIMU-type field contains samples from St. Helena (Chaffey et al., 1989; Willbold and Stracke, 2006), Walvis–Mocamedes (including Agate Mountain; Homrighausen et al., 2018a; Homrighausen et al., 2018b; this study), Gibeon (Davies et al., 2001), Dicker Willem (this study), Vema seamount (Class and le Roex, 2011), Swakopmund (this study) and Richardson–South Africa track (Homrighausen et al., 2018b; Homrighausen et al., 2020 and references therein). Two samples from the continental part of the Richardson–South Africa track show $^{208}Pb/^{204}Pb$ and $^{143}Nd/^{144}Nd$ ratios distinct from the HIMU-type field, indicating contamination by continental crust and thus were not plotted.

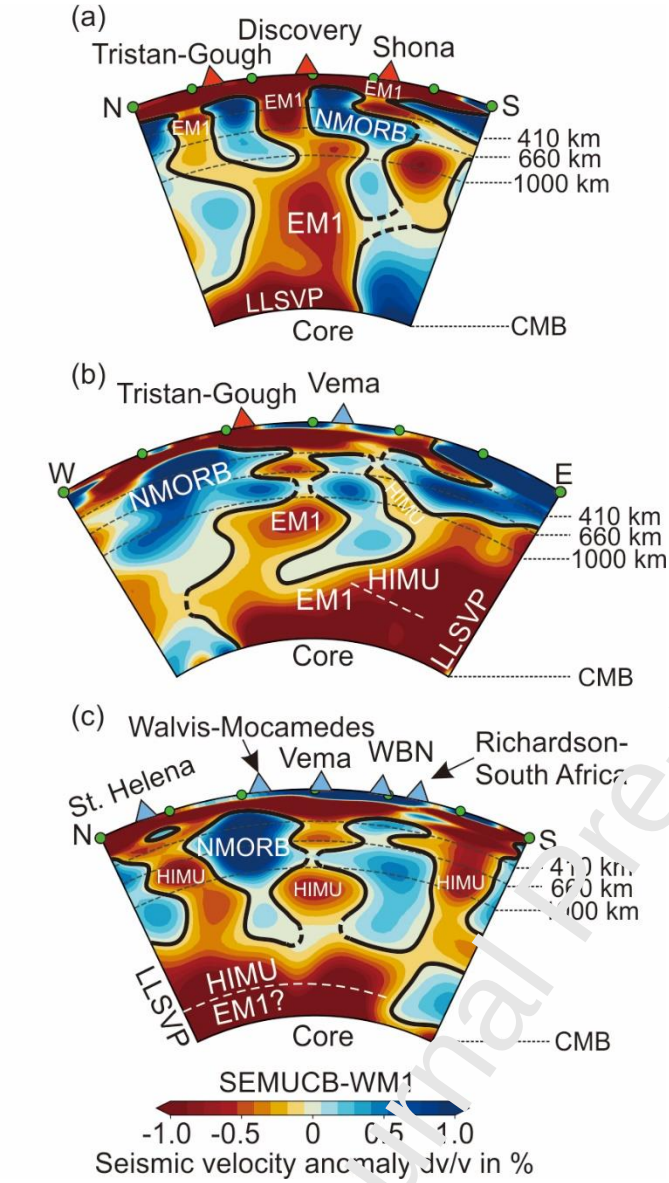

Figure 9: Seismic tomographic profiles using velocity model SEMUCB-WM1 (French and Romanowicz, 2014) through today's mantle (see Figure 1 for profile locations): (a) N-S profile through the mantle beneath Tristan-Gough, Discovery and Shona (EM1-type) hotspots, (b) E-W profile through Tristan-Gough (EMI-type) and VEMA–Gibbeon (HIMU-type) hotspots, and (c) N-S profile through St. Helena, Walvis–Mocamedes, Vema–Gibbeon, Warmbad-Bushmanland-Namaqualand (WBN) and Richardson–South Africa (HIMU-type) hotspots. Profile (a) shows a large low-velocity anomaly rising from the westernmost margin

of the Large Low-Shear Velocity Province (LLSVP), which forms three distinct branches (arms) between ~1000-2000 km that can be traced to the base of the three EM1-type hotspots: Tristan-Gough, Discovery and Shona. Profile (b) shows near continuous low-velocity anomalies ascending from the LLSVP to the base of the lithosphere beneath the SW end of the Tristan-Gough hotspot track and the Vema seamount. Profile (c) shows a continuous low-velocity anomaly extending from an internal, shallower portion of the LLSVP to the base of the lithosphere beneath St. Helena and the Richardson–South Africa HIMU volcanic tracks and a near continuous low-velocity anomaly ascending beneath the Walvis–Mocamedes, Swakopmund, Vema–Dicker Willem–Gibbon and the WBN HIMU volcanic tracks. The low-velocity anomalies are interpreted as mantle plumes derived from the outer margin (EMI-type) and from an inner (~900-1200km east) step (HIMU-type) of the LLSVP. Figures produced with the SubMachine software (Hosseini et al., 2018). Abbreviations: NMORB = normal mid-Atlantic ridge basalt; WBN = Warmbad, Bushmanland and Namaqualand volcanism; CMB = Core mantle boundary.

References

Baby, G., Guillocheau, F., Morin, J., Ressouche, J., Robin, C., Broucke, O., Dall'Asta, M., 2018. Post-rift stratigraphic evolution of the Atlantic margin of Namibia and South Africa: Implications for the vertical movements of the margin and the uplift history of the South African Plateau. Marine and Petroleum Geology 97, 169-191.

Ballmer, M.D., Schumacher, L., Lekic, V., Thomas, C., Ito, G., 2016. Compositional layering within the large low shear-wave velocity provinces in the lower mantle. Geochem. Geophys. Geosyst. 17, 5056-5077.

Bell, K., Tilton, G., 2001. Nd, Pb and Sr isotopic compositions of East African carbonatites: evidence for mantle mixing and plume inhomogeneity. J. Petrol. 42, 1927-1945.

Blichert-Toft, J., Chauvel, C., Albarède, F., 1997. Separation of Hf and Lu for high-precision isotope analysis of rock samples by magnetic sector-multiple collector ICP-MS. Contrib. Mineral. Petrol. 127, 248-260.

Burke, K., Steinberger, B., Torsvik, T.H., Smethurst, M.A., 2008. Plume Generation Zones at the margins of Large Low Shear Velocity Provinces on the core–mantle boundary. Earth Planet. Sci. Lett. 265, 49-60.

Campeny, M., Kamenetsky, V.S., Melgarejo, J.C., Mangas, J., Manuel, J., Alfonso, P., Kamenetsky, M.B., Bambi, A.C.J.M., Gonçalves, A.O., 2015. Carbonatitic lavas in Catanda (Kwanza Sul, Angola): Mineralogical and geochemical constraints on the parental melt. Lithos 232, 1-11.

Castillo, P.R., 2015. The recycling of marine carbonates and sources of HIMU and FOZO ocean island basalts. Lithos 216-217, 254-263.

Castillo, P.R., Liu, X., Scarsi, P., 2020. The geochemistry and Sr-Nd-Pb isotopic ratios of high 3He/4He Afar and MER basalts indicate a significant role of the African Superplume in EARS magmatism. Lithos 376, 105791.

Chaffey, D., Cliff, R., Wilson, B., 1989. Characterization of the St Helena magma source. Geological Society, London, Special Publications 42, 257-276.

Chauvel, C., Maury, R.C., Blais, S., Lewin, E., Guillou, H., Guille, G., Rossi, P., Gutscher, M.-A., 2012. The size of plume heterogeneities constrained by Marquesas isotopic stripes. Geochem. Geophys. Geosyst. 13, n/a-n/a.

Cheng, Z., Zhang, Z., Hou, T., Santosh, M., Chen, L., Ke, S., Xu, L., 2017. Decoupling of Mg–C and Sr–Nd–O isotopes traces the role of recycled carbon in magnesiocarbonatites from the Tarim Large Igneous Province. Geochim. Cosmochim. Acta 202, 159-178.

Class, C., Lehnert, K., 2012. PetDB Expert MORB (Mid-Ocean Ridge Basalt) Compilation, Version1.0. Interdisciplinary Earth Data Alliance (IEDA). https://doi .org /10 .1594 /IEDA /100060.

Class, C., le Roex, A., 2011. South Atlantic DUPAL anomaly — Dynamic and compositional evidence against a recent shallow origin. Earth Planet. Sci. Lett. 305, 92-102.

Class, C., le Roex, A.P., 2006. Continental material in the shallow oceanic mantle—How does it get there? Geology 34, 129.

Cooper, A., 1988. Geology of Dicker Willem, a subvolcanic carbonatite complex in south-west Africa. Comm. GeoI. Surv. SW Afr./Namibia 4, 3-12.

Cooper, A., Reid, D., 2000. The association of potassic trachytes and carbonatites at the Dicker Willem Complex, southwest Namibia: coexisting, immiscible, but not cogenetic magmas. Contrib. Mineral. Petrol. 139, 570-583.

Cooper, A.F., Reid, D.L., 1998. Nepheline sövites as parental magmas in carbonatite complexes: evidence from Dicker Willem, southwest Namibia. J. Petrol. 39, 2123-2136.

Dasgupta, R., Hirschmann, M.M., 2006. Melting in the Earth's deep upper mantle caused by carbon dioxide. Nature 440, 659-662.

Dasgupta, R., Hirschmann, M.M., Smith, N.D., 2007. Partial Melting Experiments of Peridotite + CO2 at 3 GPa and Genesis of Alkalic Ocean Island Basalts. J. Petrol. 48, 2093-2124.

Davies, G., Spriggs, A., Nixon, P., 2001. A non-cognate origin for the Gibeon kimberlite megacryst suite, Namibia: implications for the origin of Namibian kimberlites. J. Petrol. 42, 159-172.

Ernst, R.E., Bell, K., 2010. Large igneous provinces (LIPs) and carbonatites. Mineral. Petrol. 98, 55-76.

French, S., Romanowicz, B., 2014. Whole-mantle radially anisotropic shear velocity structure from spectral-element waveform tomography. Geophysical Journal International 199, 1303-1327.

Frimmel, H.E., Lane, K., 2005. Geochemistry of carbonate beds in the Neoproterozoic Rosh Pinah Formation, Namibia: Implications on depositional setting and hydrothermal ore formation. South African Journal of Geology 108, 5-18.

Garbe-Schönberg, C.D., 1993. Simultaneous determination of thirty - seven trace elements in twenty - eight international rock standards by ICP - MS. Geostandards and Geoanalytical Research 17, 81-97.

Garbe-Schönberg, D., Müller, S., 2014. Nano-particulate pressed powder tablets for LA-ICP-MS. J. Anal. At. Spectrom. 29, 990-1000.

Govindaraju, K., 1994. 1994 compilation of working values and sample description for 383 geostandards. Geostandards and Geoanalytical Research 18, 1-158.

Gudfinnsson, G.H., Presnall, D.C., 2005. Continuous Gradations among Primary Carbonatitic, Kimberlitic, Melilititic, Basaltic, Picritic, and Komatiitic Melts in Equilibrium with Garnet Lherzolite at 3–8 GPa. J. Petrol. 46, 1645-1659.

Hoernle, K., Abt, D.L., Fischer, K.M., Nichols, H., Hauff, F., Abers, G.A., Van Den Bogaard, P., Heydolph, K., Alvarado, G., Protti, M., 2008. Arc-parallel flow in the mantle wedge beneath Costa Rica and Nicaragua. Nature 451, 1094.

Hoernle, K., Hauff, F., Kokfelt, T.F., Haase, K., Garbe-Schönberg, D., Werner, R., 2011. On- and off-axis chemical heterogeneities along the South Atlantic Mid-Ocean-Ridge (5–11° S): Shallow or deep recycling of ocean crust and/or intraplate volcanism? Earth Planet. Sci. Lett. 306, 86-97.

Hoernle, K., Rohde, J., Hauff, F., Garbe-Schönberg, D., Homrighausen, S., Werner, R., Morgan, J.P., 2015. How and when plume zonation appeared during the 132 Myr evolution of the Tristan Hotspot. Nat. Commun. 6, 7799.

Hoernle, K., Schwindrofska, A., Werner, R., van den Bogaard, P., Hauff, F., Uenzelmann-Neben, G., Garbe-Schönberg, D., 2016. Tectonic dissection and displacement of parts of Shona hotspot volcano 3500 km along the Agulhas-Falkland Fracture Zone. Geology 44, 263-266.

Hoernle, K., Tilton, G., Le Bas, M.J., Duggen, S., Garbe-Schönberg, D., 2002. Geochemistry of oceanic carbonatites compared with continental carbonatites: mantle recycling of oceanic crustal carbonate. Contrib. Mineral. Petrol. 142, 520-542.

Hofmann, A.W., 1988. Chemical differentiation of the Earth: the relationship between mantle, continental crust, and oceanic crust. Earth Planet. Sci. Lett. 90, 297-314.

Homrighausen, S., Hoernle, K., Geldmacher, J., Wartho, J.-A., Hauff, F., Portnyagin, M., Werner, R., van den Bogaard, P., Garbe-Schönberg, D., 2018a. Unexpected HIMU-type late-stage volcanism on the Walvis Ridge. Earth Planet. Sci. Lett. 492, 251-263.

Homrighausen, S., Hoernle, K., Hauff, F., Geldmacher, J., Wartho, J.-A., van den Bogaard, P., Garbe-Schönberg, D., 2018b. Global distribution of the HIMU end member: Formation through Archean plume-lid tectonics. Earth-Science Reviews 182, 85-101.

Homrighausen, S., Hoernle, K., Hauff, F., Wartho, J.-A., van den Bogaard, P., Garbe-Schönberg, D., 2019. New age and geochemical data from the Walvis Ridge: The temporal and spatial diversity of South Atlantic intraplate volcanism and its possible origin. Geochim. Cosmochim. Acta 245, 16-34.

Homrighausen, S., Hoernle, K., Zhou, H., Geldmacher, J., Wartho, J.-A., Hauff, F., Werner, R., Jung, S., Morgan, J.P., 2020. Paired EMI-HIMU hotspots in the South Atlantic—Starting plume heads trigger compositionally distinct secondary plumes? Science Advances 6, eaba0282.

Hosseini, K., Matthews, K.J., Sigloch, K., Shephard, G.E., Domeier, M., Tsekhmistrenko, M., 2018. SubMachine: Web - based tools for exploring seismic tomography and other models of Earth's deep interior. Geochem. Geophys. Geosyst. 19, 1464-1483.

Janney, P., 2007. Sr-Nd-Pb-Hf isotope geochemistry of mafic alkaline igneous rocks from the Gibeon Dicker Willem lineament, southern Namibia. AGUFM 2007, V13D-1590.

Jochum, K.P., Garbe - Schönberg, D., Veter, M., Stoll, B., Weis, U., Weber, M., Lugli, F., Jentzen, A., Schiebel, R., Wassenburg, J.A., 2019. Nano - powdered calcium carbonate reference materials: Significant progress for microanalysis? Geostandards and Geoanalytical Research 43, 595-609.

Keller, J., Hoefs, J., 1995. Stable Isotope Characteristics of Recent Natrocarbonatites from Oldoinyo Lengai, in: Bell, K., Keller, J. (Eds.), Carbonatite Volcanism: Oldoinyo Lengai and the Petrogenesis of Natrocarbonatites. Springer Berlin Heidelberg, Berlin, Heidelberg, pp. 113-123.

Le Bas, M., Streckeisen, A.L., 1991. The IUGS systematics of igneous rocks. Journal of the Geological Society 148, 825-833.

Le Maitre, R., Bateman, P., Dudek, A., Keller, J., Lameyre, J., Le Bas, M., Sabine, P., Schmid, R., Sorensen, H., Streckeisen, A., 1989. A classification of igneous rocks and glossary of terms. Recommendations of the IUGS Subcommission on the Systematics of Igneous rocks. London: Blackwell Scientific Publications.

Le Maitre, R.W., Streckeisen, A., Zanettin, B., Le Bas, M., Bonin, B. Bateman, P., 2005. Igneous rocks: a classification and glossary of terms: recommendations of the International Union of Geological Sciences Subcommission on the Systematics of Igneous Rocks. Cambridge University Press.

le Roex, A., Class, C., 2014. Metasomatism of the Pan-African lithospheric mantle beneath the Damara Belt, Namibia, by the Tristan mantle plume: geochemical evidence from mantle xenoliths. Contrib. Mineral. Petrol. 168.

Le Roex, A.P., Lanyon, R., 1998. Isotope and Trace Element Geochemistry of Cretaceous Damaraland Lamprophyres and Carbonatites, Northwestern Namibia: Evidence for Plume—Lithosphere Interactions. J. Petrol. 39, 1117-1146.

Marsh, J., Ewart, A., Milner, S., Duncan, A., Miller, R.M., 2001. The Etendeka Igneous Province: magma types and their stratigraphic distribution with implications for the evolution of the Paraná-Etendeka flood basalt province. Bulletin of Volcanology 62, 464-486.

Marsh, J., Phillips, D., Lock, B., 2018. $^{40}Ar/^{39}Ar$ dating of the Klinghardt and Stalhart Phonolites, Namibia, and Comments on the Evolution of the Klinghardt Volcanic Field. Communications of the Geological Survey of Namibia 20, 1-8.

Martin, L.H., Schmidt, M.W., Mattsson, H.B., Guenther, D., 2013. Element partitioning between immiscible carbonatite and silicate melts for dry and H2O-bearing systems at 1–3 GPa. J. Petrol. 54, 2301-2338.

Mather, B.R., Müller, R.D., Seton, M., Ruttor, S., Nebel, O., Mortimer, N., 2020. Intraplate volcanism triggered by bursts in slab flux. Science advances 6, eabd0953.

Mazza, S.E., Gazel, E., Bizimis, M., Moucha, R., Beguelin, P., Johnson, E.A., McAleer, R.J., Sobolev, A.V., 2019. Sampling the volatile-rich transition zone beneath Bermuda. Nature 569, 398-403.

McDermott, F., Hawkesworth, C., 1990. Intracrustal recycling and upper-crustal evolution: a case study from the Pan-African Damara mobile belt, central Namibia. Chem. Geol. 83, 263-280.

Miller, R.M., 2000. The Agate Mountain Carbonatite Complex, Cape Fria, NW Namibia. communs geol. Surv. Namibia 12, 369-382.

Miller, R.M., 2008. The geology of Namibia. Ministry of Mines and Energy, Geological Survey.

Milner, S.C., Le Roex, A.P., Watkins, R.T., 1993. Rb-Sr age determinations of rocks from the Okenyenya igneous complex, northwestern Namibia. Geological Magazine 130, 335-343.

Münker, C., Pfänder, J.A., Weyer, S., Büchl, A., Kleine, T., Mezger, K., 2003. Evolution of planetary cores and the Earth-Moon system from Nb/Ta systematics. Science 301, 84-87.

Nakamura, Y., Tatsumoto, M., 1988. Pb, Nd, and Sr isotopic evidence for a multicomponent source for rocks of Cook-Austral Islands and heterogeneities of mantle plumes. Geochim. Cosmochim. Acta 52, 2909-2924.

Nascimento, D.B., Schmitt, R.S., Ribeiro, A., Trouw, R.A., Passchier, C.W., Basei, M.A., 2017. Depositional ages and provenance of the Neoproterozoic Damara Supergroup (northwest Namibia): Implications for the Angola-Congo and Kalahari cratons connection. Gondwana Research 52, 153-171.

O'Connor, J.M., le Roex, A.P., 1992. South Atlantic hot spot-plume systems: 1. Distribution of volcanism in time and space. Earth Planet. Sci. Lett. 113, 343-364.

Ray, J.S., Pande, K., Bhutani, R., Shukla, A.D., Rai, V.K., Kumar, A., Awasthi, N., Smitha, R., Panda, D.K., 2013. Age and geochemistry of the Newania dolomite carbonatites, India: implications for the source of primary carbonatite magma. Contrib. Mineral. Petrol. 166, 1613-1632.

Reid, D., Cooper, A., Rex, D., Harmer, R., 1990. Timing of post–Karoo alkaline volcanism in southern Namibia. Geological Magazine 127, 427-433.

Richards, M.A., Duncan, R.A., Courtillot, V.E., 1989. Flood basalts and hot-spot tracks: plume heads and tails. Science 246, 103-107.

Rohde, J., Hoernle, K., Hauff, F., Werner, R., O'Connor, J., Class, C., Garbe-Schonberg, D., Jokat, W., 2013. 70 Ma chemical zonation of the Tristan-Gough hotspot track. Geology 41, 335-338.

Rooney, T.O., Nelson, W.R., Dosso, L., Furman, T., Hanan, B., 2014. The role of continental lithosphere metasomes in the production of HIMU-like magmatism on the northeast African and Arabian plates. Geology 42, 419-422.

Sarda, P., Moreira, M., Staudacher, T., Schilling, J.G., Allègre, C.J., 2000. Rare gas systematics on the southernmost Mid - Atlantic Ridge: Constraints on the lower mantle and the Dupal source. Journal of Geophysical Research: Solid Earth 105, 5973-5996.

Schwindrofska, A., Hoernle, K., Hauff, F., van den Bogaard, P., Werner, R., Garbe-Schönberg, D., 2016. Origin of enriched components in the South Atlantic: Evidence from 40 Ma geochemical zonation of the Discovery Seamounts. Earth Planet. Sci. Lett. 441, 167-177.

Stracke, A., Hofmann, A.W., Hart, S.R., 2005. FOZO, HIMU, and the rest of the mantle zoo. Geochem. Geophys. Geosyst. 6, n/a-n/a.

Strganac, C., Salminen, J., Jacobs, L.L., Polcyn, M.J., Ferguson, K.M., Mateus, O., Schulp, A.S., Morais, M.L., da Silva Tavares, T., Gonçalves, A.O., 2014. Carbon isotope stratigraphy, magnetostratigraphy, and 40Ar/39Ar age of the Cretaceous South Atlantic coast, Namibe Basin, Angola. Journal of African Earth Sciences 99, 452-462.

Stroncik, N.A., Trumbull, R.B., Krienitz, M.-S., Niedermann, S., Romer, R.L., Harris, C., Day, J., 2017. Helium isotope evidence for a deep-seated mantle plume involved in South Atlantic breakup. Geology 45, 827-830.

Sun, S.-S., McDonough, W.F., 1989. Chemical and isotopic systematics of oceanic basalts: implications for mantle composition and processes. Geological Society, London, Special Publications 42, 313-345.

Trumbull, R., 2004. Oxygen and neodymium isotope evidence for source diversity in Cretaceous anorogenic granites from Namibia and implications for A-type granite genesis. Lithos 73, 21-40.

U.S. Geological Survey, 2020, Mineral commodity summaries 2020: U.S. Geological Survey, 200 p., https://doi.org/10.3133/mcs2020.

Walter, M.J., Bulanova, G.P., Armstrong, L.S., Keshav, S., Blundy, J.D., Gudfinnsson, G., Lord, O.T., Lennie, A.R., Clark, S.M., Smith, C.B., Gobbo, L., 2008. Primary carbonatite melt from deeply subducted oceanic crust. Nature 454, 622-625.

Weidendorfer, D., Manning, C.E., Schmidt, M.W., 2020. Carbonate melts in the hydrous upper mantle. Contrib. Mineral. Petrol. 175, 1-17.

Whitehead, K., Le Roex, A., Class, C., Bell, D., 2002. Composition and Cretaceous thermal structure of the upper mantle beneath the Damara Mobile Belt: evidence from nephelinite-hosted peridotite xenoliths, Swakopmund, Namibia. Journal of the Geological Society 159, 307-321.

Willbold, M., Stracke, A., 2006. Trace element composition of mantle end - members: Implications for recycling of oceanic and upper and lower continental crust. Geochem. Geophys. Geosyst. 7.

Woodhead, J.D., 1996. Extreme HIMU in an oceanic setting: The geochemistry of Mangaia Island (Polynesia), and temporal evolution of the Cook—Austral hotspot. J. Volcanol. Geotherm. Res. 72, 1-19.

Yang, K.-F., Fan, H.-R., Santosh, M., Hu, F.-F., Wang, K.-Y., 2011. Mesoproterozoic carbonatitic magmatism in the Bayan Obo deposit, Inner Mongolia, North China: Constraints for the mechanism of super accumulation of rare earth elements. Ore Geology Reviews 40, 122-131.

Zhou, H., Hoernle, K., Geldmacher, J., Hauff, F., Garbe-Schönberg, D., Jung, S., Bindeman, I., 2022. Enriched mantle one (EMI) type carbonatitic volcanism in Namibia: Evidence for a concentrically-zoned Etendeka plume head. Gondwana Research 109, 239-252.

Zhou, H., Hoernle, K., Geldmacher, J., Hauff, F., Homrighausen, S., Garbe-Schönberg, D., Jung, S., 2020. Geochemistry of Etendeka magmatism: Spatial heterogeneity in the Tristan-Gough plume head. Earth Planet. Sci. Lett. 535, 116123.

Declaration of interests

☒ The authors declare that they have no known competing financial interests or personal relationships that could have appeared to influence the work reported in this paper.

☐The authors declare the following financial interests/personal relationships which may be considered as potential competing interests:

A HIMU-like volcanism belt along the southwest Africa.

The HIMU-like volcanic complexes form age-progressive volcanic tracks.

EMI and HIMU mantle plumes are from different domains in the lower mantle.